1. Extended Data

Complete the Inventory below for all Extended Data figures.

Figure #	Figure title One sentence only	Filename This should be the name the file is saved as when it is uploaded to our system. Please include the file extension. i.e.: *Smith_ED_Fig1.jpg*	Figure Legend If you are citing a reference for the first time in these legends, please include all new references in the Online Methods References section, and carry on the numbering from the main References section of the paper.
Extended Data Fig. 1	**Correlation between transversal and longitudinal MSOT collagen$_{mean/max}$ signals**	Regensburger_ ED_Fig1.jpg	Each independent muscle was analyzed for its transversal and longitudinal MSOT collagen$_{mean}$ (**a**) and collagen$_{max}$ (**b**) signal. Correlations between longitudinal and transversal MSOT collagen$_{mean/max}$ signals are given by Spearman correlation coefficient (r_s). Two-tailed test. Linear regression lines are in black. P values ≤0.05 were considered statistically significant. n = 316 muscle regions (n = 159 transversal/n = 157 longitudinal independent muscle regions) in n = 20 biologically independent subjects (n = 10 HV/n = 10 DMD patients).
Extended Data Fig. 2	**Standard B-mode ultrasound imaging**	Regensburger_ ED_Fig2.jpg	Representative examples of transversal and longitudinal B-mode ultrasound imaging of quadriceps femoris muscles in a HV and in a patient with DMD. A representative result for a HV and a DMD from n = 160 independent muscle regions (n = 80 HV/n = 80 DMD) of n = 20 biologically independent subjects (n = 10 HV/n = 10 DMD patients) with similar results is shown. Scale bars, 1cm.
Extended Data Fig. 3	**Quantification of 2D and 3D MSOT collagen$_{max}$ signals in WT and DMD muscles over time**	Regensburger_ ED_Fig3.jpg	Quantification of 2D (**a**) and 3D (**b**) MSOT collagen$_{max}$ signals in WT and DMD piglet muscles over time. WT and DMD MSOT collagen$_{max}$ signals of independent piglet muscles of all animals were compared with each other at weeks 1, 2, 3, and 4 of age. Each filled circle represents one MSOT signal per independent muscle region (n =

			24 WT/n = 20 DMD). Two-tailed independent samples t-tests (with Welch's correction in cases of unequal variances) was used for statistical analysis. If the assumption of normal distribution was violated, a Mann-Whitney U-test was used. P values ≤ 0.05 were considered statistically significant. Bonferroni-Holm adjustment was used to control type I error, due to four comparisons (week 1 - 4) per parameter (e.g. 2D collagen$_{mean}$). Confidence intervals (95%CI), effect size (R^2), coefficients (t(df)/U) and exact p values are noted in the main text and/or Supplementary Tables. Data are shown as mean ± SD. n = 44 independent muscle regions (n = 24 WT/n = 20 DMD) in n = 11 biologically independent animals (n = 6 WT/n = 5 DMD piglets) from n = 2 litters are shown.
Extended Data Fig. 4	**Quantification of 2D and 3D MSOT collagen$_{max}$ signals in WT and DMD piglet muscles over time**	Regensburger_ ED_Fig4.jpg	2D (**a**) and 3D (**b**) MSOT collagen$_{max}$ signals of independent piglet muscles of surviving animals were compared with each other at weeks 1, 2, 3, and 4 of age. Each filled circle/square represents the mean ± SD MSOT signal of independent muscle regions over the course of the experiment (n = 12WT/n = 8 DMD). 2D MSOT parameters were analyzed by post-hoc Tukey's HSD following a mixed-effects models due to missing values in week 1 (litter 1). p values ≤ 0.05 were considered statistically significant. 3D MSOT collagen parameters were analyzed by Tukey's honestly significant difference tests following a two-way (mixed design) ANOVA; Data are shown as mean ± SD. n = 20 independent muscle regions (n = 12 WT/n = 8 DMD) in n = 5 biologically independent animals (n = 3 WT/n = 2 DMD piglets) from n = 2 litters are shown.
Extended Data Fig. 5	**Overview of independent muscle regions in each DMD piglet over time**	Regensburger_ ED_Fig5.jpg	2D (**a, b**) and 3D (**c, d**) MSOT collagen$_{mean/max}$ signals of each independent muscle region of all surviving DMD piglets over the course of the experiment. Each icon represents one independent muscle over the time period,

			connected by a colored line (weeks 1, 2, 3, and 4 of age). SR, shoulder right (yellow line); LR, leg right (blue line); SL, shoulder left (purple line); LL, leg left (green line). n = 8 independent muscle regions (n = 4 in DMD-number-2/n = 4 in DMD-number-5) of n = 2 biologically independent animals (n = 2 DMD piglets) from n = 2 litters are shown.
Extended Data Fig. 6	**Overview of the mean MSOT collagen$_{mean/max}$ signals per individual piglet over time**	Regensburger_ED_Fig6.jpg	Mean 2D (**a, b**) and mean 3D (**c, d**) MSOT collagen$_{mean/max}$ signals per individual piglet over time (weeks 1, 2, 3, and 4 of age). Each filled circle represents the mean ± SD MSOT signal of an independent piglet over the course of the experiment (n = 6WT/n = 5 DMD). n = 11 biologically independent animals (n = 6WT/n = 5 DMD piglets) from n = 2 litters are shown.
Extended Data Fig. 7	**Standardization and positioning of the detector probe**	Regensburger_ED_Fig7.jpg	Examples of detector probe positioning and MSOT scanning. Exact positioning of the MSOT detector was standardized for each anatomical region (Supplementary Table 23) and marked with small labels (e.g. red dots). Scanning of a 3-year-old volunteer with the 2D MSOT detector is presented.

Delete rows as needed to accommodate the number of figures (10 is the maximum allowed).

2. Supplementary Information:

A. Flat Files

Complete the Inventory below for all additional textual information and any additional Supplementary Figures, which should be supplied in one combined PDF file.

Item	Present?	Filename This should be the name the file is saved as when it is uploaded	A brief, numerical description of file contents. i.e.: *Supplementary Figures 1-4, Supplementary*

		to our system, and should include the file extension. The extension must be .pdf	*Discussion, and Supplementary Tables 1-4.*
Supplementary Information	Yes	2_Supplementary Appendix_V2.0.pdf	Supplementary Tables 1-23
Reporting Summary	Yes	reportingsummary_1572018146_5.pdf	

B. Additional Supplementary Files

Complete the Inventory below for all additional Supplementary Files that cannot be submitted as part of the Combined PDF.

Type	Number If there are multiple files of the same type this should be the numerical indicator. i.e. "1" for Video 1, "2" for Video 2, etc.	Filename This should be the name the file is saved as when it is uploaded to our system, and should include the file extension. i.e.: *Smith_Supplementary_Video_1.mov*	Legend or Descriptive Caption Describe the contents of the file
Supplementary Video		NatMed_MSOT_DMD.mov	**Video – Real-time 2D MSOT imaging in newborn piglets** The video shows a halved screen. On the left side live imaging of a piglet is presented. The detector was placed on the thigh (biceps femoris muscle) of the piglet. The right video shows simultaneous MSOT imaging. Spectral unmixing for collagen (turquoise) and lipids (yellow) is overlaid to RUCT images. A

			representative video for MSOT real-time imaging from n = 58 independent muscle regions (n = 34 WT/n = 24 DMD) in n = 17 biologically independent animals (n = 10 WT/n = 7 DMD piglets) from n = 3 litters with similar results is shown.

Add rows as needed to accommodate the number of files.

3. Source Data

Complete the Inventory below for all Source Data files.

Figure	Filename This should be the name the file is saved as when it is uploaded to our system, and should include the file extension. i.e.: *Smith_SourceData_Fig1.xls*, or *Smith_Unmodified_Gels_Fig1.pdf*	Data description i.e.: Unprocessed Western Blots and/or gels, Statistical Source Data, etc.
Source Data Fig. 1	Source_Data_Fig_1.xlsx	Statistical Source Data
Source Data Fig. 2	Source_Data_Fig_2.xlsx	Statistical Source Data
Source Data Fig. 3	Source_Data_Fig_3.xlsx	Statistical Source Data
Source Data Fig. 4	Source_Data_Fig_4.xlsx	Statistical Source Data
Source Data Fig. 5	Source_Data_Fig_5.xlsx	Statistical Source Data
Source Data Fig. 6	Source_Data_Fig_6.xlsx	Statistical Source Data
Source Data Fig. 7		
Source Data Fig. 8		
Source Data Extended Data Fig. 1	Source_Data_Extended_Data_Fig_1.xlsx	Statistical Source Data
Source Data Extended Data Fig. 2		
Source Data	Source_Data_Extended_Dat	Statistical Source Data

Extended Data Fig. 3	a_Fig_3.xlsx	
Source Data Extended Data Fig. 4	Source_Data_Extended_Data_Fig_4.xlsx	Statistical Source Data
Source Data Extended Data Fig. 5	Source_Data_Extended_Data_Fig_5.xlsx	Statistical Source Data
Source Data Extended Data Fig. 6	Source_Data_Extended_Data_Fig_6.xlsx	Statistical Source Data

Detection of collagens by multispectral optoacoustic tomography as an imaging biomarker for Duchenne muscular dystrophy

Adrian P. Regensburger, M.D.[1], Lina M. Fonteyne, D.V.M.[2], Jörg Jüngert, M.D.[1], Alexandra L. Wagner, M.D.[1], Teresa Gerhalter, PhD[3,4,5], Armin M Nagel, PhD[3,4,5], Rafael Heiss, M.D.[3], Florian Flenkenthaler, PhD[2], Matthias Qurashi[6], Markus F. Neurath, M.D.[6,7], Nikolai Klymiuk, PhD[2], Elisabeth Kemter, D.V.M.[2], Thomas Fröhlich, PhD[2], Michael Uder, M.D.[3], Joachim Woelfle, M.D.[1], Wolfgang Rascher, M.D.[1], Regina Trollmann, M.D.[1], Eckhard Wolf, D.V.M.[2], Maximilian J. Waldner, M.D.[6,8†], and Ferdinand Knieling, M.D.[1†*]

[1] Department of Pediatrics and Adolescent Medicine, University Hospital Erlangen, Friedrich-Alexander-Universität Erlangen-Nürnberg (FAU), Erlangen, Germany
[2] Institute for Molecular Animal Breeding and Biotechnology, and Laboratory for Functional Genome Analysis (LAFUGA), Gene Center, Ludwig-Maximilian-University Munich, Munich, Germany
[3] Institute of Radiology, University Hospital Erlangen, Friedrich-Alexander-Universität Erlangen-Nürnberg (FAU), Erlangen, Germany
[4] Institute of Medical Physics, Friedrich-Alexander-Universität Erlangen-Nürnberg (FAU), Erlangen, Germany
[5] Division of Medical Physics in Radiology, German Cancer Research Center (DKFZ), Heidelberg, Germany
[6] Department of Medicine 1, University Hospital Erlangen, Friedrich-Alexander-Universität Erlangen-Nürnberg (FAU), Erlangen, Germany

[7] Ludwig Demling Center of Excellence, Friedrich-Alexander-Universität Erlangen-Nürnberg (FAU), Erlangen, Germany
[8] Erlangen Graduate School in Advanced Optical Technologies (SAOT), Friedrich-Alexander-Universität Erlangen-Nürnberg (FAU), Erlangen, Germany

† shared authorship

* **Corresponding author**

Ferdinand Knieling, M.D.
Pediatric Experimental and Translational Imaging Laboratory (PETI-Lab)
Department of Pediatrics and Adolescent Medicine
University Hospital Erlangen
Friedrich-Alexander-University of Erlangen-Nürnberg
Loschgestraße 15
91054 Erlangen, Germany

Phone: +49 9131 85-33118
Fax: +49 9131 85-33113
Mail: Ferdinand.Knieling@uk-erlangen.de

Abstract

Biomarkers for monitoring disease progression and response to therapy are lacking for muscle diseases such as Duchenne muscular dystrophy. Non-invasive *in vivo* molecular imaging with multispectral optoacoustic tomography (MSOT) utilizes pulsed laser light to induce acoustic pressure waves, enabling the visualization of endogenous chromophores. Here, we describe a novel application of MSOT, in which illumination in the near- and extended near-infrared range (NIR and exNIR) from 680-1100 nm enables the visualization and quantification of collagen content. We first demonstrated the feasibility of this approach to non-invasively quantify tissue fibrosis in longitudinal studies in a large-animal DMD model in pigs, and then applied this approach to pediatric patients (NCT03490214). MSOT-derived collagen content measurements in skeletal muscle were highly correlated to the functional status of the patients and provided additional information on molecular features as compared to magnetic resonance imaging. This study highlights the potential of MSOT imaging as a non-invasive, age-independent biomarker for the implementation and monitoring of newly-developed therapies in muscular diseases.

Introduction

Duchenne muscular dystrophy (DMD) is the most common lethal inherited X-chromosomal muscular disease occurring in one of 3,800-6,000 live male births [1]. Initially, affected boys develop normally, but at the age of four to five years loss of functional muscle mass becomes apparent. Within a few years, relevant muscle and tendon shortening lead to muscular weakness resulting in loss of ambulation around the age of ten, finally ending in respiratory and cardiac failure in the third decade. DMD is caused by loss-of-function mutations in the dystrophin gene leading to dystrophin deficiency and resulting in muscular degeneration, followed by inflammation and fatty and fibrotic transformation [2-4]. Promising new therapeutic approaches aiming to restore disturbed molecular mechanisms by enabling the ribosomal read-through of premature stop codons [5,6] or exon skipping [7] have been approved, and others such as viral gene therapy, utrophin modulators [8] and CRISPR/Cas-mediated correction of *DMD* mutations provide promising early results [9]. Until now, primary outcome measures are based on manual [10] and quantitative muscle examinations [11] as well as timed function tests [5-7,12]. Furthermore, magnetic resonance imaging (MRI) [13-15] and magnetic resonance spectroscopy (MRS) [16-18] have shown potential as non-invasive imaging techniques for quantification of disease pathology and progression in DMD. However, these and other techniques have limited applicability due to considerable acquisition times [14,18], a required sedation in early childhood and uncooperative patients, as well as the effort towards nationwide availability of novel standardized imaging protocols [19]. Until now, a standardized 6-minute walk test (6-MWT) is one of the main primary outcome measures to assess the effects of pharmaceutical interventions [5-7,20,21]. However, physical examinations rely on active cooperation and the individual performance on the day, which might limit their diagnostic validity. To overcome an unmet clinical need for independent

easy-to-apply prognostic biomarkers [22] and to enable guidance for earliest therapeutic interventions during infancy, novel non-invasive diagnostic approaches are required. Multispectral Optoacoustic Tomography (MSOT) is an emerging imaging modality capable of non-invasively visualizing the distribution of endogenous absorbers by initiating laser-induced thermoelastic expansion and detection of resulting pressure waves [23,24]. Further, the clinical usability for the detection of endogenous molecular chromophores, such as (de-)oxygenated hemoglobin, oxygen saturation, and melanin has already been demonstrated in melanoma lymph nodes [25], breast cancer [26,27], melanoma [28] and chronic intestinal inflammation [29,30]. The utilization of wavelengths in the extended near-infrared range (exNIR) would also enable the visualization of lipids and collagens [31-36]. This report provides the first insight into how MSOT using exNIR illumination is capable of visualizing fibrotic muscular transformation *in vivo* suggesting its application as a novel non-invasive imaging biomarker in muscular dystrophy.

Results

NIR/exNIR MSOT imaging detects and separates collagen signals

MSOT uses spectral unmixing to identify different endogenous chromophores **(Fig. 1a)**. To prove the unmixing algorithm and signal separation for collagens, a custom-made phantom was built. First, solutions of purified human collagens (I, III, and IV) were imaged every 5 nm from 660-1200 nm. The separated optoacoustic spectra of each collagen peaked similarly between 980 and 1000 nm, clearly distinguishable from hemoglobin, lipid, and water signals (**Fig. 1b**). For further validation, normalized spectra of *ex vivo* porcine tendons (mainly collagen I), collagen I solutions, and the spectra derived from literature [31] were compared. Therefore, a region of

interest (ROI) was outlined in the reflective ultrasound computed tomography (RUCT), which is used to anatomically guide the investigator during imaging (**Fig. 1c).** When using a translatable setup limited to a maximum of 11 wavelengths (680, 700, 730, 760, 800, 850, 920, 1000, 1030, 1064, and 1100 nm**, Fig. 1c**) the collagen spectra of the tendon and the purified collagen I resembled those reported in the literature (collagen peak at ~1000 nm) (**Fig. 1c**) [31] . Furthermore, *in vivo* imaging of tendons was carried out, confirming our spectral unmixing approach, by showing specific unmixed collagen signals mainly within the tendon (**Fig. 1d**).

Collagen detection in a porcine DMD model

Subsequently, 2D MSOT imaging was performed in a translational porcine model of DMD (**Fig. 2a and Supplementary Video**). In total n = 58 scans from independent muscle regions (n = 34 in wild type piglets (WT)/n = 24 in DMD piglets) were acquired from n = 17 piglets (n = 10 WT/n = 7 DMD). Using ultrasound guidance, a region of interest (ROI) was drawn within the examined muscle to quantify the MSOT parameters, such as the mean and the maximum collagen signals ($collagen_{mean/max}$). Initially, all independent muscle regions were compared between groups (n = 34 WT/n = 24 DMD muscles). A significant difference for the $collagen_{mean/max}$ signal was observed ($collagen_{mean}$: 14.41 ± 2.66 a.u. vs. 23.14 ± 3.87 a.u., p = $1.18x10^{-11}$, t(df) = 9.57 (38), 95%CI 6.88 - 10.57, R^2 = 0.71; $collagen_{max}$: 27.68 ± 2.72 a.u. vs. 41.05 ± 7.43 a.u., p = 4.38 x 10^{-9}, (df) = 8.43 (27), 95%CI 10.12 - 16.63, R^2 = 0.72). Second, when comparing a mean collagen signal per independent piglet between groups (n = 10WT/n = 7 DMD piglets), the $collagen_{mean/max}$ signals were similarly increased ($collagen_{mean}$: 14.23 ± 1.96 a.u. vs. 22.67 ± 3.59 a.u., p = 1.51 x 10^{-5}, (df) = 6.27 (15), 95%CI 5.57 - 11.31, R^2 = 0.72; $collagen_{max}$: 27.70 ± 1.67 a.u. vs. 41.01 ± 5.16 a.u., p = 1.39 x 10^{-6}, (df) = 7.69 (15), 95%CI

59.62 - 17.00, $R^2 = 0.80$). There was no difference in signal levels of deoxygenated (Hb_R), oxygenated (HbO_2) and total hemoglobin (Hb_{total}) ($p > 0.05$, **Fig. 2b and Supplementary Table 1 and 2**).

An exploratory receiver operator characteristic (ROC) analysis revealed excellent ability of MSOT-derived collagen signals to distinguish healthy from diseased muscles (n = 34 WT/n = 24 DMD muscle regions) ($collagen_{mean}$: AUC 0.98, 95%CI 0.95 - 1.00, $p = 6.06 \times 10^{-10}$; $collagen_{max}$: AUC 0.98, 95%CI 0.96 - 1.00, $p = 4.96 \times 10^{-10}$, **Fig. 2c**). Corresponding tissue specimens were taken for validation in which *ex vivo* histopathology revealed muscular dystrophy and a qualitative increase in collagen formation in diseased animals (**Fig. 2d**). In total, n = 18 WT muscles of n = 6 piglets and n = 12 DMD muscles of n = 3 piglets were analyzed quantitatively by the positive stained collagen area on Trichrome (TriC) and Sirius Red (SirR) stained histological sections or the ratio between total collagen and total protein (TC/TP). One WT muscle could not be histologically quantified. All corresponding analyses showed significant differences between the cohorts suggesting elevated values in DMD piglets (means: TriC: 5.35% vs. 12.63%, $p = 4.08 \times 10^{-5}$, (df) = 5.59 (16), 95%CI 4.52 - 10.05, $R^2 = 0.66$; SirR: 8.44% vs. 16.23%, p = 0.0003, (df) = 4.56 (16), 95%CI 4.17 - 11.39, $R^2 = 0.56$; and TC/TP: 46.83 µg collagen/mg protein vs. 64.95 µg collagen/mg protein, p = 0.0240, (df) = 2.39 (28), 95%CI 2.56 - 33.68, $R^2 = 0.19$, respectively, **Fig. 2e-g**). Additionally, highly significant correlations to MSOT collagen signals were found (TriC: $r_s = 0.58$, p = 0.0010, 95%CI 0.26 - 0.78, SirR: $r_s = 0.65$, p = 0.0001, 95%CI 0.37 - 0.83 and TC/TP: $r_s = 0.53$, p = 0.0027, 95%CI 0.20 - 0.75, respectively, **Fig. 2e-g**).

Two-dimensional collagen detection in DMD patients and healthy volunteers

To study our approach in patients, we enrolled n = 10 DMD patients and n = 10 age- and gender-matched healthy volunteers (HV) in a first-in pediatric trial. Mean age of affected boys was 7.1 ± 1.6 years and 7.3 ± 2.2 years in matched HV (detailed clinical data is shown in the **Supplementary Table 3**).

In total N = 320 scans (transversal and longitudinal scans of eight muscles per participant) were obtained. N = 4 scans were excluded for the following reasons: N = 1 broken scan, N = 3 region of interest (ROI) was beyond the depth limit of the detector (below 3.5 cm). The average scan time for 2D and 3D images was 6.3 ± 0.8 min in DMD patients and 6.7 ± 0.6 min in HV.

Exemplary *in vivo* imaging (**Fig. 3a**) and transversal images of a single HV and DMD patient are presented in **Fig. 3b,** illustrating a qualitative difference of collagen signal intensity in every muscle region between both groups. In accordance with our preclinical model, each independent muscle was analyzed for its $collagen_{mean/max}$ signal. High correlations between transversal and longitudinal $collagen_{mean}$ and $collagen_{max}$ signals were found (**Extended Data Fig. 1**). Therefore, only transversal images were used for further analyses. All independent muscle regions (n = 80 HV/n = 79 DMD muscles), showed statistically significant differences between both groups for 2D MSOT $collagen_{mean/max}$ (age-matched n =79 independent muscle regions; $collagen_{mean}$: 14.60 ± 4.42 a.u. vs. 24.72 ± 5.92 a.u., $p < 1.0 \times 10^{-15}$, 95%CI 8.50 - 11.76, t(df) = 12.37(78), $R^2 = 0.66$ and $collagen_{max}$: 26.55 ± 6.16 a.u. vs. 40.52 ± 7.71 a.u., $p < 1.0 \times 10^{-15}$, 95%CI 10.40 - 16.28, $W^- = -17$).

Considering the mean $collagen_{mean/max}$ signal per independent subject between groups (n = 10 HV/n = 10 DMD patients), significant differences in matched comparison of the mean ($collagen_{mean}$: 14.59 ± 2.52 a.u. vs. 24.70 ± 2.77 a.u., $p = 1.78 \times 10^{-5}$, 95%CI 7.33 -1 2.90, t(df) = 8.22(9), $R^2 = 0.88$) and the maximum collagen content ($collagen_{max}$: 26.59 ± 3.51 a.u. vs. 40.48 ±

206 3.81 a.u., $p = 5.17 \times 10^{-6}$, 95%CI 10.61 - 17.18, t(df) = 9,57(9), $R^2 = 0.91$) were found (**Fig. 3c**).
207 There was no significant difference found in lipid, Hb_R, HbO_2 and Hb_{total} signals between both
208 groups (**Supplementary Table 4)**. ROC analysis of n = 80 HV/n = 79 DMD independent muscle
209 regions suggested good diagnostic performance for 2D $collagen_{mean}$ (AUC 0.92, 95%CI 0.88 -
210 0.96, $p < 1.0 \times 10^{-15}$) and 2D $collagen_{max}$ (AUC 0.92, 95%CI 0.88 - 0.96, $p < 1.0 \times 10^{-15}$) to
211 distinguish healthy from diseased muscles (**Fig. 3d**).

212

213 **Three-dimensional MSOT imaging in DMD patients and healthy volunteers**
214 Furthermore, we aimed to prove a volumetric (3D) MSOT imaging approach. A total of N = 160
215 3D scans from independent muscle regions (n = 80 HV/n = 80 DMD muscles) were acquired.
216 The 3D detector is designed as a cup (**Fig. 4a**) and operates at higher frequencies (8 MHz)
217 compared to the 2D detector (4 MHz). The heavy water couplet and a thinner detector foil,
218 enable a high resolution and a clear visualization of subcutaneous chromophores (**Fig. 4b**).
219 Similar to our 2D analysis approach, 3D data sets demonstrated a significant difference of the
220 $collagen_{mean/max}$ signal in all anatomical independent muscle regions (age-matched n =80
221 independent muscle regions, n = 80 HV/n = 80 DMD: $collagen_{mean}$ 5.39 ± 2.20 a.u. vs 11.41 ±
222 2.10 a.u., $p < 1.0 \times 10^{-15}$, 95%CI 5.28 - 6.76, t(df) = 16.09(79), $R^2 = 0.77$ and $collagen_{max}$ 12.94 ±
223 2.95 a.u. vs 23.66 ± 6.46 a.u., $p < 1.0 \times 10^{-15}$, 95%CI 7.60 - 10.90, $W^- = -2$). The mean
224 $collagen_{mean/max}$ signal for each independent subject were analyzed and showed significant
225 differences (age-matched n = 10 HV and n = 10 DMD patients: $collagen_{mean}$ 5.39 ± 0.80 a.u. vs
226 11.41 ± 1.01 a.u., $p = 9.99 \times 10^{-8}$, 95%CI 5.13 - 6.92, t(df) = 15.2(9), $R^2 = 0.96$ and $collagen_{max}$
227 12.94 ± 1.19 a.u. vs 23.66 ± 3.28 a.u., $p = 2{,}01 \times 10^{-5}$, 95%CI 7.73 - 13.72, t(df) = 8.1(9), R^2 =
228 0.88). In contrast to the scans using the 2D detector, there were significant differences in the

optoacoustic signals for Hb_R, HbO_2 and Hb_{total} using 3D-detection. In DMD subjects, Hb_R, HbO_2 and Hb_{total} were significantly decreased (**Fig. 4c and Supplementary Table 5**). The mean collagen content was inversely correlated with Hb_R (n = 20 independent patients (n = 10HV/n = 10DMD; mean signal): r_s = -0.60, p = 0.0051, 95%CI -0.83 - (-0.20)), HbO_2 (n = 20 independent patients (n = 10 HV/n = 10 DMD, mean signal): r_s = -0.81, p = 1.67 x 10^{-5}, 95%CI -0.92 - (-0.56)) and Hb_{total} (n = 20 independent patients (n = 10 HV/n = 10 DMD, mean signal): r_s = -0.81, p = 1.78 x 10^{-5}, 95%CI -0.92 - (-0.56)) contents of the muscle. ROC analysis demonstrated excellent diagnostic performance of the 3D approach to distinguish healthy from diseased muscles (independent muscle regions of n = 80 HV/n = 80 DMD patients: $collagen_{mean}$: AUC 0.98, 95%CI 0.97 - 1.00, p < 1.0 x 10^{-15} and $collagen_{max}$: AUC 0.98, 95%CI 0.96 - 1.00, p < 1.0 x 10^{-15}) (**Fig. 4d**).

MSOT has significant correlation to clinical standard assessments

Every participant (N = 20) underwent a standardized physical examination. Except the time for a single rise from chair and muscle strength of the upper/lower distal extremities, all timed function tests and manual muscle testing, showed significant between-group differences (**Supplementary Table 3**). Notably, not all patients were able to complete all tests, due to cognitive impairment, fatigue, or state of distraction.

Significant negative correlations between every mean MSOT $collagen_{mean/max}$ signal and the 6-MWT were found (n = 20 independent subjects (n = 10 HV/n = 10 DMD): $collagen_{2D\text{-}mean}$ r_s = -0.74, p = 0.0002, 95%CI -0.89 - (-0.42); $collagen_{2D\text{-}max}$ r_s = -0.69, p = 0.0007, 95%CI -0.87 - (-0.35); $collagen_{3D\text{-}mean}$ r_s = -0.64, p = 0.0023, 95%CI -0.85 - (-0.26); $collagen_{3D\text{-}max}$ r_s = -0.71, p = 0.0005, 95%CI -0.88 - (-0.38)). The other timed function tests showed similar consistent

correlation with collagen signals, except single rise from chair and MRC of the lower distal extremity. No correlation with age was observed (e.g. $collagen_{2D\text{-}mean}$ r_s = -0.06, p = 0.79, 95%CI -0.50 - 0.40); , **Fig. 5a and Supplementary Table 6**). In addition, comparison of MSOT collagen signals between the thigh and lower leg in DMD patients showed no overall significant differences (**Supplementary Table 7**). In comparison to MSOT, a total of n = 320 standard ultrasound B-mode images (n = 160 transversal/n = 160 longitudinal images) were evaluated (**Extended Data Figure 2**). Only transversal scans were used for statistical analyses. Independent muscles of HV (n = 80) and DMD patients (n = 80) showed different echogenicity, texture, and scores on Heckmatt scale (**Supplementary Table 8**). A negative correlation between the mean MSOT 2D $collagen_{mean}$ and muscle echogenicity (Spearman r_s = -0.53, 6.08 x 10^{-13}, 95% CI -0.63 - (-0.41)), and a significant positive correlation between MSOT collagen and Heckmatt scale (Spearman r_s = 0.38, 9.39 x 10^{-7}, 95% CI 0.23 - 0.51, **Supplementary Table 9**) were found. During all MSOT investigations, ultrasound, and physical examinations, no serious adverse events were reported (**Supplementary Table 10**).

For further comparison, n = 5 DMD patients underwent MRI of the right lower leg (**Fig. 5b**). Total scan time was between 60 and 75 minutes. The time interval between MRI and MSOT imaging was 2.4 ± 1.34 months (for details see **Supplementary Table 11)**. No significant correlation was found between MSOT $collagen_{mean}$ (n = 5 DMD patients) and fat fraction (FF), water T_2, total tissue sodium concentration (TSC), and intracellular-weighted sodium signal (ICwS), respectively. However, TSC and ICwS content measured by MRI and collagen signals derived by MSOT showed a correlation but were not significant (r_s = 0.70, p = 0.23, 95% CI n/a), respectively) (**Supplementary Table 12**). Noteworthy, the patient with the highest FF (FF of

0.374) showed the highest 2D MSOT lipid (920 nm) signal (**Fig. 5b and Supplementary Table 11**).

MSOT quantitatively visualizes early-stage disease progression

To demonstrate the feasibility of our approach for the *in vivo* monitoring of disease progression in DMD, a longitudinal study in the DMD piglet model was conducted (**Fig. 6a**). From initial n = 11 male piglets, n = 5 completed the full experimental protocol and were sacrificed after 4 times consecutive weekly MSOT imaging. n = 3 DMD piglets died early for different reasons; thus n = 3 corresponding WT piglets were sacrificedll other animals were sacrificed after imaging procedures in week 4. (**Fig. 6b**). n = 44 independent muscles (biceps and triceps muscle of both sides, **Fig 6c**) (n = 24 WT/n = 20 DMD) were investigated in week 1, and n = 20 independent muscles (n = 12 WT/n = 8 DMD) were imaged through the whole experiment. *In vivo* MSOT imaging revealed visible tissue changes in the DMD piglets over time by means of increased fibrotic transformation (**Fig. 6d**). Again, a significant MSOT collagen$_{mean/max}$ signal difference (2D and 3D) was found in all independent muscle regions of WT (n = 24 in week 1/n = 12 in week 2, 3, and 4) and DMD (n = 20 in week 1/n = 8 in week 2, 3, and 4) piglets compared between every week of the experiment (**Fig. 6e**, **Extended Data Fig. 3**, **Supplementary Table 13 and Supplementary Table 14**). Comparison of the independent muscle regions (n = 12 WT/n = 8 DMD) of the preserving n = 5 piglets (n = 3 WT/n = 2 DMD) showed a steady increase of 2D and 3D MSOT collagen signals only in DMD over the time course of four weeks (**Fig. 6e, Extended Data Fig. 4-6, Supplementary Tables 15-18**). At week 4, the end of the study, the differences between both cohorts were clearly evident *in vivo*, *ex vivo* macroscopically, and histologically (**Fig. 6f and 6g**). In the DMD cohort, histological and

bioanalytical collagen quantification demonstrated an increased collagen deposition within four weeks up to 248% (TriC %, week 1 to week 4: 10.40 ± 5.14 to 25.80 ± 7.93, $p = 4.94 \times 10^{-5}$, t(df) = 5.29 (18), 95%CI 9.29-21.51, $R^2 = 0.61$) and 170% (SirR %, week 1 to week 4: 19.59 ± 5.40 to 33.30 ± 5.71, $p = 3.63 \times 10^{-5}$, t(df) = 5.43 (18), 95%CI 8.41 - 19.01, $R^2 = 0.62$) from baseline, respectively. Collagen per protein content quantification increased up to 139% (TC/TP µg/mg week 1 to week 4: 77.57 ± 38.80 to 107.80 ± 42.02, p = 0.12, t(df) = 1.65 (18), 95%CI -8.24 - 68.63, $R^2 = 0.13$) (**Fig. 6h**).

To further confirm muscular fibrosis and the potential origin of MSOT signals, quantitative proteome analysis was performed on n = 16 snap-frozen independent tissue samples (n = 8 WT/n = 8 DMD) of n = 8 independent piglets (n = 4 WT/n = 4 DMD), showing clear separation of proteomes according to age and genotype (**Fig. 6i-k**). In total, 2820 proteins were identified **(Fig. 6k)**. Comparing collagens between WT and DMD piglets, collagen VI (COL6A1, 1.7-fold; COL6A2 1.6-fold; COL6A3, 1.7-fold) was already enriched in DMD piglets in week one of life. In the fourth week of life, besides the most abundant collagen VI, collagen III and collagen XIV were also increased (COL3A1, 6.3-fold; COL14A1, 1.6-fold) (**Supplementary Table 19 and Supplementary Table 20**).

Discussion

This translational approach suggests a potential role for MSOT as a novel *in vivo* contrast-agent free and non-invasive imaging modality for the quantitative detection of collagen as a biomarker in DMD.

In our previous work, we already demonstrated the capability of MSOT in near infrared range (NIR) for disease monitoring in Crohn’s disease by detecting different signal levels of

hemoglobin as markers of intestinal inflammatory activity[29,30]. To date, the utilization of wavelengths in the extended near-infrared range (exNIR) has so far only been reported in experimental settings[28,32,35,36] but, to the best of our knowledge, has never been applied in a clinical trial – especially not in pediatrics.

Our findings suggest that quantitative assessment of collagen content in muscles with MSOT is a suitable method for monitoring of degeneration involving fibrotic processes *in vivo*, as shown in this study in a large animal model and a pediatric cohort. The extracted collagen spectra were in agreement with previously reported optoacoustic spectra [31,33-35]; visualization and quantification of collagen was feasible in all anatomical regions and showed significant differences between diseased and healthy animals as well as in the human cohorts. Accelerated disease progression in DMD piglets leading to early structural changes[37] might explain comparable results of animal and human findings in this study.

Currently, several new treatments for DMD are under investigation, but until now, there is an unmet need for established objective monitoring techniques and age-independent biomarkers in clinical practice [13,22]. So far, the 6-MWT is the most commonly used primary endpoint for disease assessment in DMD but essentially requires active patient compliance [5-7,20,21]. The complexity to accurately execute these tests and the dependence on cooperative behavior limit the significance of muscular function tests to more adolescent patients. Most recent trials were restricted to DMD patients aged over 5-7 years [5-7], which prohibits conclusions on early therapeutic interventions. In comparison to established imaging modalities like ultrasound imaging [38,39] and MRI [40-43], MSOT is a target-specific quantitative, non-invasive, bedside imaging modality. MRI is still limited by long image-acquisition times and requires immobilization and, in early childhood, sedation. In our study, we demonstrated that MSOT can

be performed in subjects down to 3 years of age, while minimal scan times (<7min for 8 anatomical regions) suggest that it could even be performed from birth.

MRI protocols are further limited for detecting fibrosis specifically, since signal alterations in T2-weighted, water-sensitive MRI images are nonspecific, due to the sensitivity to inflammation, edema, fibrosis, as well as necrosis and the influence of corticosteroid treatments [43]. MRI has shown potential for treatment monitoring [42,43], and emerging protocols like ^{23}Na MRI might even add further value [18,42,44]. The latter enables detection of increased sodium content, which potentially also reflects elevated glycosaminoglycans (GAGs) [45] and extracellular matrix (ECM) production [46,47]. The similarities between increased MRI TSC and MSOT collagen content in our study points towards an overlapping depiction of enriched ECM in DMD patients [48]. However, the conclusions drawn in our study regarding MRI TSC are limited by the small sample size and the heterogeneity of the DMD collective.

The slightly divergent imaging outcomes for the 2D and 3D detector might reflect different technical designs of the detectors used in our study. The differences of deoxygenated and oxygenated hemoglobin content of the muscle between HV and DMD patients and the negative correlation of hemoglobin and collagens is in line with the pathophysiological mechanism of muscular degeneration underlying DMD [4]. Notably, fatty transformation could not be unequivocally detected using MSOT, most likely due to the high absorption of the subcutaneous fat tissue compared to the relatively low fat fraction (< 10%) within the muscles of four of the five investigated participants. However, this also reflects the findings in previous reports where combined peri- and endomysial fibrosis were exceeding 30% [49], while intramuscular fat content in similar aged DMD biceps femoris and quadriceps femoris muscle ranged only from 0.89 ±

0.70% [50] to 3.4 ± 4.1% [49], respectively. In this regard, fatty infiltration is known to be distributed very heterogeneously within single muscles of DMD patients [51,52].

Dating the initiation of skeletal muscle degeneration back to intrauterine life [53,54], Peverelli et al. observed increased connective tissue proportions of 16.5% in one-year-old DMD patients compared to 3% in healthy subjects, rapidly peaking to 30% and more in the following years [49,50,55,56]. These findings support our concept to consider fibrosis as an early imaging target in DMD.

As this was the first-in pediatric use of multispectral optoacoustic imaging, this study was limited in scope and size. Nevertheless, 320 2D scans and 160 3D scans were recorded in this exploratory study, which underlines the ability of MSOT as a highly specific and sensitive tool for potential disease monitoring in DMD. Excellent imaging precision[57], as well as reproducibility and repeatability[58] have been shown previously. We have demonstrated an age-independent, significant negative correlation between MSOT collagen parameters and the clinical muscle function. Considering results from our longitudinal experiments, MSOT might be suitable to perform follow-up studies or therapeutic monitoring. As described in 3-month-old DMD piglets [59], we now validated our longitudinal imaging results by proving the increase in muscular fibrosis and increased abundance of ECM proteins (e.g. collagens) even at the age of four weeks.

Novel therapeutic approaches leading to an ultrastructural restoration of damaged muscles [60] might therefore be directly visualized using MSOT in future studies. While our findings remain preliminary, our approach starting with experimental tissues and progressing through to first in-patient application supports MSOT-derived collagen detection and quantification as a potential

387 age-independent imaging biomarker for disease progress monitoring in DMD and suggest the
388 potential for further applications.
389

Acknowledgements

F.K. acknowledges founding from Else Kröner–Fresenius–Stiftung (Else Kröner-Memorial-Stipendium, 2018_EKMS.03). A.P.R. received support from the ELAN Fond at the University Hospital of the Friedrich-Alexander-Universität (FAU) Erlangen-Nürnberg. F.K. and A.P.R. acknowledge support by the Interdisciplinary Center for Clinical Research (IZKF) at the University Hospital of the Friedrich-Alexander-Universität (FAU) Erlangen-Nürnberg. A.M.N. acknowledges funding from Johannes and Frieda Marohn Foundation. MJW received support from the Graduate School in Advanced Optical Technologies of the Friedrich-Alexander-Universität (FAU) Erlangen-Nürnberg. MFN acknowledges funding from the Emerging Fields Initiative (EFI) of the Friedrich-Alexander-Universität (FAU) Erlangen-Nürnberg. M.J.W and MFN acknowledge founding from German Research Foundation (FOR2438, TRR241). E.W. acknowledges funding from Else Kröner-Fresenius Foundation (2015_180; 2018_T20), Bayerische Forschungsstiftung (AZ 802/08) and German Research Foundation (TRR127). M.F.N., M.J.W., F.K. received funding from the European Union's Horizon 2020 research and innovation programme under grant agreement No 830965. We thank the Imaging Science Institute (Erlangen, Germany) for providing us with the measurement time at the 3 T MRI system. The present work was performed in partial fulfillment of the requirements for obtaining the degree „Dr. med. vet." (LMF). We thank the patients and healthy volunteers who committed their time and effort. We grateful acknowledge our physiotherapists Jutta Tolks, Martina Müller-Allissat and Patricia Poepperl for excellent assistance and physical testing of the participants. We thank the administrative staff at the Center for Social Pediatrics and the Center for Rare Neuromuscular Diseases within the Center for Rare Disease at the University Hospital Erlangen with a special thanks to Stephanie Schuessler, M.D. for help during patient recruitment, Gudrun

Boie and Ida Allabauer for performing histological techniques, Christina Blechinger for exceptional help during animal husbandry and histological preparations, Benjamin Marty, PhD, for fruitful discussions about MRI in muscular diseases. Guy Poland, D.V.M., for language editing and Matthias Englbrecht, PhD, for statistical review of the manuscript.

Author contributions

R.T. and F.K. conceived the idea of the study. Phantom imaging was performed by A.P.R., A.L.W. and F.K. A.P.R., R.T., M.J.W., and F.K. designed the study and recruited the pediatric participants. R.T., M.J.W. and F.K. were the principal investigators of the pediatric study. Ultrasound imaging was performed by J.J. M.Q. provided device support. The animal model was designed by E.W. and N.K. The animal studies were designed by A.P.R., L.M.F., E.W., M.J.W. and F.K. E.W. was the principal investigator of the animal study and A.P.R., L.M.F., A.L.W., and F.K. performed the imaging studies. Pediatric MSOT imaging was performed by A.P.R. and F.K. Human MRI imaging was performed and analyzed by T.G., A.M.N., R.H., A.P.R. and M.U. *Ex vivo* tissue analyses were performed by L.M.F., E.K., A.P.R. and F.K. T.F. and F.F. performed mass spectrometry. Data collection was completed and analyzed by A.P.R. and F.K. A.P.R., L.M.F., M.F.N., E.W., T.G., W.R., J.W., M.J.W., and F.K. interpreted the data. A.P.R. and F.K. wrote the first draft of the manuscript. The manuscript was critically reviewed by all authors.

Competing interests

A.P.R., M.J.W., F.K. are co-inventors together with iThera Medical GmbH, Germany on an EU patent application (EP 19 163 304.9) relating to a device and a method for analyzing

optoacoustic data, a optoacoustic system and a computer program. A.P.R., M.J.W., and F.K. received travel support by iThera Medical GmbH, Germany. F.K. reports lecture fees from Siemens Healthcare GmbH outside the submitted work. All other authors declare no competing interests.

References

1. Mendell, J.R. & Lloyd-Puryear, M. Report of MDA muscle disease symposium on newborn screening for Duchenne muscular dystrophy. *Muscle Nerve* **48**, 21-26 (2013).
2. Mercuri, E. & Muntoni, F. Muscular dystrophies. *Lancet* **381**, 845-860 (2013).
3. Hoffman, E.P., Brown, R.H., Jr. & Kunkel, L.M. Dystrophin: the protein product of the Duchenne muscular dystrophy locus. *Cell* **51**, 919-928 (1987).
4. Klingler, W., Jurkat-Rott, K., Lehmann-Horn, F. & Schleip, R. The role of fibrosis in Duchenne muscular dystrophy. *Acta Myol* **31**, 184-195 (2012).
5. Bushby, K., *et al.* Ataluren treatment of patients with nonsense mutation dystrophinopathy. *Muscle Nerve* **50**, 477-487 (2014).
6. McDonald, C.M., *et al.* Ataluren in patients with nonsense mutation Duchenne muscular dystrophy (ACT DMD): a multicentre, randomised, double-blind, placebo-controlled, phase 3 trial. *Lancet* **390**, 1489-1498 (2017).
7. Mendell, J.R., *et al.* Longitudinal effect of eteplirsen versus historical control on ambulation in Duchenne muscular dystrophy. *Ann Neurol* **79**, 257-271 (2016).
8. Fairclough, R.J., Wood, M.J. & Davies, K.E. Therapy for Duchenne muscular dystrophy: renewed optimism from genetic approaches. *Nat Rev Genet* **14**, 373-378 (2013).
9. Klymiuk, N., *et al.* Tailored Pig Models for Preclinical Efficacy and Safety Testing of Targeted Therapies. *Toxicol Pathol* **44**, 346-357 (2016).
10. Brooke, M.H., *et al.* Clinical investigation in Duchenne dystrophy: 2. Determination of the "power" of therapeutic trials based on the natural history. *Muscle Nerve* **6**, 91-103 (1983).
11. Escolar, D.M., *et al.* Randomized, blinded trial of weekend vs daily prednisone in Duchenne muscular dystrophy. *Neurology* **77**, 444-452 (2011).
12. Mayhew, J.E., *et al.* Reliable surrogate outcome measures in multicenter clinical trials of Duchenne muscular dystrophy. *Muscle Nerve* **35**, 36-42 (2007).
13. Straub, V., *et al.* Stakeholder cooperation to overcome challenges in orphan medicine development: the example of Duchenne muscular dystrophy. *Lancet Neurol* **15**, 882-890 (2016).
14. Willcocks, R.J., *et al.* Multicenter prospective longitudinal study of magnetic resonance biomarkers in a large duchenne muscular dystrophy cohort. *Ann Neurol* **79**, 535-547 (2016).
15. Weber, M.A., *et al.* Permanent muscular sodium overload and persistent muscle edema in Duchenne muscular dystrophy: a possible contributor of progressive muscle degeneration. *J Neurol* **259**, 2385-2392 (2012).
16. Wary, C., *et al.* Quantitative NMRI and NMRS identify augmented disease progression after loss of ambulation in forearms of boys with Duchenne muscular dystrophy. *NMR Biomed* **28**, 1150-1162 (2015).
17. Hooijmans, M.T., *et al.* Elevated phosphodiester and T2 levels can be measured in the absence of fat infiltration in Duchenne muscular dystrophy patients. *NMR Biomed* **30**(2017).
18. Gerhalter, T., *et al.* (23) Na MRI Depicts Early Changes in Ion Homeostasis in Skeletal Muscle Tissue of Patients With Duchenne Muscular Dystrophy. *J Magn Reson Imaging* (2019).
19. Forbes, S.C., *et al.* Skeletal muscles of ambulant children with Duchenne muscular dystrophy: validation of multicenter study of evaluation with MR imaging and MR spectroscopy. *Radiology* **269**, 198-207 (2013).
20. McDonald, C.M., *et al.* The 6-minute walk test in Duchenne/Becker muscular dystrophy: longitudinal observations. *Muscle Nerve* **42**, 966-974 (2010).
21. McDonald, C.M., *et al.* The 6-minute walk test as a new outcome measure in Duchenne muscular dystrophy. *Muscle Nerve* **41**, 500-510 (2010).
22. Szigyarto, C.A. & Spitali, P. Biomarkers of Duchenne muscular dystrophy: current findings. *Degener Neurol Neuromuscul Dis* **8**, 1-13 (2018).
23. Ntziachristos, V. & Razansky, D. Molecular imaging by means of multispectral optoacoustic tomography (MSOT). *Chem Rev* **110**, 2783-2794 (2010).
24. Taruttis, A. & Ntziachristos, V. Advances in real-time multispectral optoacoustic imaging and its applications. *Nat Photonics* **9**, 219-227 (2015).
25. Stoffels, I., *et al.* Metastatic status of sentinel lymph nodes in melanoma determined noninvasively with multispectral optoacoustic imaging. *Sci Transl Med* **7**, 317ra199 (2015).

26. Diot, G., *et al.* Multispectral Optoacoustic Tomography (MSOT) of Human Breast Cancer. *Clin Cancer Res* **23**, 6912-6922 (2017).
27. Becker, A., *et al.* Multispectral optoacoustic tomography of the human breast: characterisation of healthy tissue and malignant lesions using a hybrid ultrasound-optoacoustic approach. *Eur Radiol* **28**, 602-609 (2018).
28. Rey-Barroso, L., *et al.* Visible and Extended Near-Infrared Multispectral Imaging for Skin Cancer Diagnosis. *Sensors (Basel)* **18**(2018).
29. Waldner, M.J., *et al.* Multispectral Optoacoustic Tomography in Crohn's Disease: Noninvasive Imaging of Disease Activity. *Gastroenterology* **151**, 238-240 (2016).
30. Knieling, F., *et al.* Multispectral Optoacoustic Tomography for Assessment of Crohn's Disease Activity. *N Engl J Med* **376**, 1292-1294 (2017).
31. Sekar, S.K., *et al.* Diffuse optical characterization of collagen absorption from 500 to 1700 nm. *J Biomed Opt* **22**, 15006 (2017).
32. Cao, Q., Zhegalova, N.G., Wang, S.T., Akers, W.J. & Berezin, M.Y. Multispectral imaging in the extended near-infrared window based on endogenous chromophores. *J Biomed Opt* **18**, 101318 (2013).
33. Scholkmann, F., *et al.* A review on continuous wave functional near-infrared spectroscopy and imaging instrumentation and methodology. *Neuroimage* **85 Pt 1**, 6-27 (2014).
34. Weber, J., Beard, P.C. & Bohndiek, S.E. Contrast agents for molecular photoacoustic imaging. *Nat Methods* **13**, 639-650 (2016).
35. Taroni, P., *et al.* Non-invasive optical estimate of tissue composition to differentiate malignant from benign breast lesions: A pilot study. *Sci Rep* **7**, 40683 (2017).
36. Ford, S.J., *et al.* Structural and Functional Analysis of Intact Hair Follicles and Pilosebaceous Units by Volumetric Multispectral Optoacoustic Tomography. *J Invest Dermatol* **136**, 753-761 (2016).
37. Klymiuk, N., *et al.* Dystrophin-deficient pigs provide new insights into the hierarchy of physiological derangements of dystrophic muscle. *Hum Mol Genet* **22**, 4368-4382 (2013).
38. Zaidman, C.M., Malkus, E.C. & Connolly, A.M. Muscle ultrasound quantifies disease progression over time in infants and young boys with duchenne muscular dystrophy. *Muscle Nerve* **52**, 334-338 (2015).
39. Weng, W.C., *et al.* Evaluation of muscular changes by ultrasound Nakagami imaging in Duchenne muscular dystrophy. *Sci Rep* **7**, 4429 (2017).
40. Bonati, U., *et al.* Quantitative muscle MRI: A powerful surrogate outcome measure in Duchenne muscular dystrophy. *Neuromuscul Disord* **25**, 679-685 (2015).
41. Barnard, A.M., *et al.* Skeletal muscle magnetic resonance biomarkers correlate with function and sentinel events in Duchenne muscular dystrophy. *PLoS One* **13**, e0194283 (2018).
42. Glemser, P.A., *et al.* (23)Na MRI and myometry to compare eplerenone vs. glucocorticoid treatment in Duchenne dystrophy. *Acta Myol* **36**, 2-13 (2017).
43. Arpan, I., *et al.* Examination of effects of corticosteroids on skeletal muscles of boys with DMD using MRI and MRS. *Neurology* **83**, 974-980 (2014).
44. Weber, M.A., Nagel, A.M., Jurkat-Rott, K. & Lehmann-Horn, F. Sodium (23Na) MRI detects elevated muscular sodium concentration in Duchenne muscular dystrophy. *Neurology* **77**, 2017-2024 (2011).
45. Juras, V., *et al.* Histological correlation of 7 T multi-parametric MRI performed in ex-vivo Achilles tendon. *Eur J Radiol* **82**, 740-744 (2013).
46. Frantz, C., Stewart, K.M. & Weaver, V.M. The extracellular matrix at a glance. *J Cell Sci* **123**, 4195-4200 (2010).
47. Serrano, A.L. & Munoz-Canoves, P. Regulation and dysregulation of fibrosis in skeletal muscle. *Exp Cell Res* **316**, 3050-3058 (2010).
48. Negroni, E., *et al.* Glycosaminoglycan modifications in Duchenne muscular dystrophy: specific remodeling of chondroitin sulfate/dermatan sulfate. *J Neuropathol Exp Neurol* **73**, 789-797 (2014).
49. Desguerre, I., *et al.* Endomysial fibrosis in Duchenne muscular dystrophy: a marker of poor outcome associated with macrophage alternative activation. *J Neuropathol Exp Neurol* **68**, 762-773 (2009).
50. Bettica, P., *et al.* Histological effects of givinostat in boys with Duchenne muscular dystrophy. *Neuromuscular disorders : NMD* **26**, 643-649 (2016).
51. Hooijmans, M.T., *et al.* Non-uniform muscle fat replacement along the proximodistal axis in Duchenne muscular dystrophy. *Neuromuscul Disord* **27**, 458-464 (2017).
52. Chrzanowski, S.M., *et al.* Multi-slice MRI reveals heterogeneity in disease distribution along the length of muscle in Duchenne muscular dystrophy. *Acta Myol* **36**, 151-162 (2017).

53. Emery, A.E. Muscle histology and creatine kinase levels in the foetus in Duchenne muscular dystrophy. *Nature* **266**, 472-473 (1977).
54. Toop, J. & Emery, A.E. Muscle histology in fetuses at risk for Duchenne muscular dystrophy. *Clin Genet* **5**, 230-233 (1974).
55. Peverelli, L., *et al.* Histologic muscular history in steroid-treated and untreated patients with Duchenne dystrophy. *Neurology* **85**, 1886-1893 (2015).
56. Bell, C.D. & Conen, P.E. Histopathological changes in Duchenne muscular dystrophy. *J Neurol Sci* **7**, 529-544 (1968).
57. Joseph, J., *et al.* Evaluation of Precision in Optoacoustic Tomography for Preclinical Imaging in Living Subjects. *J Nucl Med* **58**, 807-814 (2017).
58. Helfen, A., *et al.* Multispectral Optoacoustic Tomography: Intra- and Interobserver Variability Using a Clinical Hybrid Approach. *J Clin Med* **8**(2019).
59. Frohlich, T., *et al.* Progressive muscle proteome changes in a clinically relevant pig model of Duchenne muscular dystrophy. *Scientific reports* **6**, 33362 (2016).
60. Min, Y.L., *et al.* CRISPR-Cas9 corrects Duchenne muscular dystrophy exon 44 deletion mutations in mice and human cells. *Sci Adv* **5**, eaav4324 (2019).

Figure 1 – exNIR MSOT can detect collagen.

a: Schematic of the concepts underlying MSOT. MSOT is based on the photoacoustic effect: pulsed multi-wavelength laser light illuminates tissues down to 3 cm in depth. Absorption of the light by different chromophores (e.g., hemoglobin, lipids, melanin, collagens) leads to ultrasound vibrations, resulting in pressure waves that can be detected and reconstructed into images. Different chromophores can be separated by spectral unmixing based on the specific absorption and reflection properties of the emitted light. RUCT**,** reflection ultrasound computed tomography. MSP, multispectral processing.

b: Solutions of purified human collagens (I, III, and IV), hemoglobin and lipids, imaged every 5 nm from 660 - 1200 nm. Left, demonstration of the ability of MSOT to separate collagens (I, III, and IV) from hemoglobin and lipids by spectral unmixing. Right, quantification of the separated optoacoustic spectra for each chromophore. A representative result from two independent experiments with similar results is shown. Scale bar, 5mm.

c: Left, example of an *ex vivo* porcine tendon in a custom made phantom (top) and the corresponding MSOT/RUCT merged images image (bottom) showing the MSOT signal for collagen (turquoise) as color-coded map overlaid on the gray-scaled RUCT image. The region of interest (ROIs, white ellipse) is outlined in the RUCT. Right, normalized optoacoustic spectra of collagens of the *ex vivo* tendon, human purified collagen I, and a collagen spectrum from the literature [31]. A representative result from two independent experiments with similar results is shown. Scale bar, 2cm.

d: Examples of *in vivo* human tendon imaging by NIR/exNIR MSOT. MSOT/RUCT merged images show signals for de-/oxygenated hemoglobin (red/blue), lipids (yellow) and collagen (turquoise) as color-coded maps overlaid on the gray-scaled RUCT image. The MSOT collagen

signal was mainly found within the tendon, whereas lipids and hemoglobin signals mainly appeared beneath the tendon or in surrounding tissues. NIR, near-infrared range (660 – 900 nm). exNIR, extended near-infrared range (900 – 1100 nm). A representative result from two independent experiments with similar results is shown. Scale bar, 5 mm.

Figure 2 – *in vivo* 2D MSOT imaging of newborn piglets

a: Representative images of skeletal muscle from healthy (WT) (upper row) and DMD (bottom row) piglets. Regions of interest (yellow boxes) are determined in the RUCT images. Qualitative differences of spectrally unmixed optoacoustic collagen signals between WT and DMD piglets are shown in turquoise. The merged MSOT/RUCT image visualizes the collagen distribution within the muscle and the ROI, respectively. A representative result for a WT and a DMD from n = 58 independent muscle regions (n = 34 WT/n = 24 DMD) in n = 17 biologically independent animals (n = 10 WT/n = 7 DMD piglets) from n = 3 litters with similar results is shown. Scale bar, 5 mm.

b: 2D MSOT $collagen_{mean/max}$ signals, as well as 2D MSOT $Hb_{R,}$ $Hb_{O2,}$ Hb_{total} signals, from WT and DMD piglets. Each filled circle represents one MSOT signal per independent muscle region (upper row) or the mean MSOT signal per independent animal (bottom row). n = 58 independent muscle regions (n = 34 WT/n = 24 DMD) in n = 17 biologically independent animals (n = 10 WT/n = 7 DMD piglets) from n = 3 litters are shown.

c: The area under the ROC curve (AUC) and 95% confidence interval for distinguishing between muscles from DMD and WT piglets, as calculated using unmixed MSOT collagen signals ($collagen_{mean}$ and $collagen_{max}$) for n = 58 independent muscle regions (n = 34 WT/n = 24 DMD) in n = 17 biologically independent animals (n = 10 WT/n = 7 DMD piglets) from n = 3 litters are shown.

d: Representative hematoxylin & eosin (H&E), Masson's Trichrome (TriC), Sirius Red (SirR), and dystrophin (Dys1) immunohistochemistry staining from imaged WT (upper row) and DMD (bottom row) piglet musculature. DMD piglet musculature shows disrupted muscular structure (H&E staining), increased collagen content (turquoise/red), and lacking dystrophin expression

(brown). Black boxes represent areas that are shown at higher magnification in the insets. A representative result for a WT and a DMD muscle from n = 29 independent muscle specimens (n = 17 WT/n = 12 DMD) from n = 9 biologically independent animals (n = 6 WT/n = 3 DMD piglets) from n = 3 litters with similar results is shown. Scale bars, 100 µm in main micrographs and 50 µm in insets.

e-f: Quantitative tissue analyses, showing positive-stained collagen area as assessed by TriC (**e**) and SirR (**f**) staining. Correlations between the positive-stained collagen areas and the MSOT $collagen_{mean}$ signal are also shown. n = 29 independent muscle specimens (n = 17 WT/n = 12 DMD) from n = 9 biologically independent animals (n = 6 WT/n = 3 DMD piglets) from n = 3 litters.

g: Quantification of total collagen abundance in WT and DMD piglets (mean values of 46.83 µg collagen/mg protein and 64.95 µg collagen/mg protein, respectively). The correlation between collagen quantification and the MSOT $collagen_{mean}$ signal is also shown. n = 30 independent muscle specimens (n = 18 WT/n = 12 DMD) from n = 9 biologically independent animals (n = 6 WT/ n = 3 DMD piglets) from n = 3 litters.

b, e-g: Two-tailed independent samples t-tests (with Welch's correction in cases of unequal variances) was used for statistical analysis. If the assumption of normal distribution was violated, a Mann-Whitney U-test was used. P values ≤ 0.05 were considered statistically significant. No adjustment for multiple comparison was applied, due to only one single comparison per parameter. Confidence intervals (95%CI), effect size (R^2), coefficients (t(df)/U) and exact p values are noted in the main text and/or Supplementary Tables. Data are shown as mean ± SD.

e-g: Correlations are given by Spearman correlation coefficient (r_s). Two-tailed test. Linear regression lines are in black. P values ≤ 0.05 were considered statistically significant.

Figure 3 – *in vivo* 2D MSOT imaging of healthy volunteers and DMD patients

a: Example of real-time imaging of a 3-year old healthy volunteer (HV) using the 2D MSOT detector probe.

b: Representative MSOT images of transversal scans from four anatomical regions of a 7-year-old HV (left panels) as compared to those of a 5-year-old with DMD (right panels). RUCT images, obtained for anatomical guidance during the examination, are also shown. MSOT/RUCT merged images show MSOT signals for hemoglobin (red) and collagen (turquoise) as color-coded maps overlaid on the gray-scaled RUCT image. Yellow boxes indicate regions of interest that were used for signal quantification. A representative result for a HV and a DMD from n = 159 independent muscle regions (n = 80 HV/n = 79 DMD) in n = 20 biologically independent subjects (n = 10 HV/n = 10 DMD patients) with similar results is shown. Scale bar, 5 mm.

c: $Collagen_{mean/max}$ signals of the HV and DMD subjects, as measured by 2D MSOT. Each filled circle represents one MSOT signal per independent muscle region (upper row) or the mean MSOT signal per independent subject (bottom row). Two-tailed dependent samples t-tests (matched for age) was used for statistical analysis. If the assumption of normal distribution was violated Wilcoxon signed-rank tests was used. Bonferroni-Holm adjustment was used to control type I error. Confidence intervals (95%CI), effect sizes (R^2), coefficients ($t(df)/W^-$) and p values are noted in the main text and Supplementary Tables. p values ≤ 0.05 were considered statistically significant. n = 158 matched independent muscle regions (n = 79 HV/n = 79 DMD) of n = 20 biologically independent subjects (n = 10 HV/n = 10 DMD patients). Data are shown as mean ± SD.

d: ROC curves for distinguishing between DMD and HV muscles using unmixed MSOT collagen parameters ($collagen_{mean}$ and $collagen_{max}$). The area under the ROC curve (AUC) is indicated with the 95% confidence interval for distinguishing between muscles from HV and DMD patients, as calculated using unmixed MSOT collagen parameters ($collagen_{mean}$ and $collagen_{max}$) for n = 159 independent muscle

667 regions (n = 80 HV/n = 79 DMD) in n = 20 biologically independent subjects (n = 10 HV/n = 10 DMD
668 patients).
669
670

Figure 4 – *in vivo* 3D MSOT imaging of healthy volunteers and DMD patients

a: Cartoon of the handheld 3D hemispherical MSOT detector probe (8 MHz center frequency). Using the NIR (660-900nm) and exNIR (900-1100nm) spectrum of light (660-1100nm), different absorbers, such as collagens, can be detected by their specific acoustic spectra. 3D imaging allows volumetric acquisition and quantification of tissue components.

b: 3D MSOT images of the same two boys from **Fig. 3b** are shown. Top row, 7-year-old HV; bottom row, 5-year-old DMD subject. Maximum projection images of the gastrocnemius muscle in two axes (XZ and YZ) and a 3D volumetric (volume) area are depicted with color-coded maps showing Hb_{total} (red), $collagen_{mean}$ (turquoise) and lipid (yellow). Scale bar, 5 mm. A representative result for a HV and a DMD from n = 160 independent muscle regions (n = 80 HV/n = 80 DMD) in n = 20 biologically independent subjects (n = 10 HV and n = 10 DMD patients) with similar results is shown.

c: Quantification of 3D MSOT signals (Hb_R = deoxygenated hemoglobin, HbO_2 = oxygenated hemoglobin, Hb_{total} = total hemoglobin, $collagen_{mean}$, $collagen_{max}$). Each filled circle represents one MSOT signal per independent muscle region (upper row) or the mean MSOT signal per independent subject (bottom row).

Two-tailed dependent samples t-tests (matched for age) was used for statistical analysis. If the assumption of normal distribution was violated Wilcoxon signed-rank tests was used. Bonferroni-Holm adjustment was used to control type I error. Confidence intervals (95%CI), effect sizes (R^2), coefficients ($t(df)/W^-$) and p values are noted in the main text and/or Supplementary Tables. p values ≤ 0.05 were considered statistically significant. n = 160 matched independent muscle regions (n = 80 HV/n = 80 DMD) in n = 20 biologically independent subjects (n = 10 HV and n = 10 DMD patients). Data are shown as mean ± SD.

d: ROC curves for distinguishing between DMD and HV muscles using unmixed MSOT collagen parameters ($collagen_{mean}$ and $collagen_{max}$). The area under the ROC curve (AUC) is indicated with the 95% confidence interval. n = 160 independent muscle regions (n = 80 HV/n = 80 DMD) in n = 20 biologically independent subjects (n = 10 HV and n = 10 DMD patients).

Figure 5 – Correlation of MSOT imaging and clinical standard assessments

a: Correlation matrix of physical examinations, age, and mean MSOT collagen$_{mean/max}$ signals. Correlations are indicated as highly positive (dark blue), highly negative (dark red,) or white (non-significant) and Spearman correlation coefficient is given in numbers. MRC = Medical Research Council (MRC) strength grading system, UE = upper extremity, LE = lower extremity, prox. = proximal, dist. = distal, 6-MWT = 6-minute-walk-test, sit to stand= sit to stand test, and 4/8 stairs = 4/8 stairs climb. Correlations are given by Spearman correlation coefficient (r_s). Two-tailed test. Two-tailed test. Bonferroni-Holm adjustment was used to control type I error, due to four comparisons (2D/3D collagen$_{mean/max}$) per parameter (e.g. 6-MWT). P values ≤ 0.05 were considered statistically significant. n = 20 biologically independent subjects (n = 10 HV/n = 10 DMD patients). Detailed p-values and numbers (n) are presented in the **Supplementary Table 6.**

b: Representative MRI images (water T_2 map, fat fraction (FF) map, total tissue sodium concentration (TSC) map, and intracellular-weighted ^{23}Na signal (ICwS)) map of a 7-year old DMD subject, compared to corresponding transversal 2D MSOT images (dashed line is drawn around the gastrocnemius muscle region). A representative result for a DMD patient from n = 5 biologically independent subjects with similar results is shown. Scale bars, 1 cm in MRI images and 5 mm in MSOT images.

Figure 6 – MSOT quantitatively visualizes early-stage disease progression over time

a: Study outline for longitudinal monitoring of DMD piglets. Imaging was performed at weeks 1, 2, 3, and 4 of life. All piglets were sacrificed after week 4, and tissue specimens were harvested.

b: Survival of WT and DMD piglets over the time course of the experiment. Kaplan-Meier curve of WT piglets (n = 6) and DMD piglets (n = 5). Circles represent censored subjects or unexpected death of subjects.

c: Schematic indicating how standardized palpable landmarks were used to locate muscles in piglets prior to imaging, ensuring repeatability of detector placement over time. Exemplary landmarks and skinned muscles are shown. Scale bar, 10 cm.

d: Representative 3D MSOT images of one DMD piglet over 4 weeks. Color-coded maps show Hb_{total} (red), $collagen_{mean}$ (turquoise) and lipid (yellow). Scale bar, 5 mm. A representative result for a DMD piglet from n = 5 biologically independent animals (n = 3 WT/n = 2 DMD piglets) from n = 2 litters is shown.

e: Quantification of 2D and 3D MSOT $collagen_{mean}$ signals in WT and DMD piglet muscles over time. In the "All scans" graphs**,** WT and DMD MSOT $collagen_{mean}$ signals of independent piglet muscles of all animals were compared with each other at weeks 1, 2, 3, and 4 of age. Each filled circle represents one MSOT signal per independent muscle region (n = 24 WT/n = 20 DMD). Two-tailed independent samples t-tests (with Welch's correction in cases of unequal variances) was used for statistical analysis. If the assumption of normal distribution was violated, a Mann-Whitney U-test was used. P values ≤ 0.05 were considered statistically significant. Bonferroni-Holm adjustment was used to control type I error, due to four comparisons (week 1 - 4) per parameter (e.g. 2D $collagen_{mean}$). Confidence intervals (95%CI), effect size (R^2), coefficients (t(df)/U) and exact p values are noted in the main text and/or Supplementary Tables. Data are shown as mean ± SD. n = 44 independent muscle regions (n = 24 WT/n = 20 DMD) in n = 11 biologically independent animals (n = 6 WT/n = 5 DMD piglets) from n = 2 litters are shown.
In the "Completed scans" graphs, WT and DMD MSOT $collagen_{mean}$ signals of independent piglet muscles of surviving animals were compared with each other at weeks 1, 2, 3, and 4 of age. Each filled

circle/square represents the mean ± SD MSOT signal of independent muscle regions over the course of the experiment (n = 12WT/n = 8 DMD). 2D MSOT parameters were analyzed by post-hoc Tukey's HSD following a mixed-effects models due to missing values in week 1 (litter 1). p values ≤ 0.05 were considered statistically significant. 3D MSOT collagen parameters were analyzed by Tukey's honestly significant difference tests following a two-way (mixed design) ANOVA; Data are shown as mean ± SD. n = 20 independent muscle regions (n = 12 WT/n = 8 DMD) in n = 5 biologically independent animals (n = 3 WT/n = 2 DMD piglets) from n = 2 litters are shown.

f-g: A representative image of a 4 week old WT and DMD piglet (**f**) and representative low magnification views of freshly-excised unstained muscle (macroscopy), as well as TriC and SiR stained muscles, from WT and DMD piglets (**g**). Macroscopic alterations and increased fibrosis are evident in DMD versus WT muscle TriC and SirR stainings. Scale bars, 1 cm (macroscopy) and 100 µm/50 µm (histology/inserts).

h: Quantitation of the positive-stained collagen area of WT and DMD piglet muscles at weeks 1 and 4 of age, as assessed by TriC and SirR staining and collagen abundance. Two-tailed independent samples t-tests (with Welch's correction in cases of unequal variances) was used for statistical analysis. If the assumption of normal distribution was violated, a Mann-Whitney U-test was used. Bonferroni-Holm adjustment was used to control type I error, due to three comparisons per parameter (e.g. TriC). Confidence intervals (95%CI), effect sizes (R^2), degrees of freedom (t(df)/U) and p values are noted in the main text. P values ≤ 0.05 were considered statistically significant. Data are shown as mean ± SD. n = 20 independent muscle specimens (n = 12 WT/n = 8 DMD) from n = 5 biologically independent animals (n = 3 WT/n = 2 DMD) from n = 2 litters.

i-k:

Quantitative proteome analysis of skeletal muscle tissue from 1- and 4-week-old DMD and WT piglets: principal component analysis (PCA) (**i**), unsupervised hierarchical clustering of LFQ intensity values (**j**) and volcano plots of log2 fold changes (**k**). In **i**, symbols represent individual muscle samples. In **k**, the permutation-based FDR significance cutoff (< 0.05) is depicted by the black curves. Two-tailed

764 independent samples t-tests (with Welch's correction) was used for statistical analysis. No
765 adjustment for multiple comparison was applied, due to reporting as significant by a
766 permutation-based FDR estimation (FDR < 0.05). p values ≤0.05 were considered statistically
767 significant. n = 16 independent muscle specimens (n = 8 WT/n = 8 DMD) from n = 8 biologically
768 independent animals (n = 4 WT/n = 4 DMD) from n = 2 litters.

Materials and Methods

Phantom imaging

Plastic placeholders were positioned in a costume made metal mold and filled with a 2% agarose/1% lipid-deuterium oxide-gel (Agarose Standard, Roti©garose, Carl Roth GmbH + Co, KG, Karlsruhe, Germany, heavy water [Deuterium oxide], 99.9%, Sigma-Aldrich Chemie GmbH, Steinheim, Germany, and Lipofundin © MCT/LCT 20%, Braun, Melsungen, Germany). Placeholders were replaced by plastic straws filled with following chromophores: purified human collagen type I (Human Type I Atelo-Collagen Solution, 3 mg/mL, VitroCol©, Advanced Biomatrix, San Diego, USA), type III (Human Collagen Solution, Type III, 1 mg/ml ®, Advanced Biomatrix, San Diego, USA), and type IV (Collagen Type IV from human cell culture, 0.3mg/ml, Sigma-Aldrich Chemie GmbH, Steinheim, Germany), anticoagulated (citrated) blood, lipids (rapeseed oil), and water.

For tissue imaging, a plastic container was filled one half with 2% agarose-gel (~~2%~~Agarose, NEEO ultra-quality, Carl Roth GmbH + Co, KG, Karlsruhe, Germany). The sample was positioned on the surface of the hardened agarose. The gel suppressed reflections on the back wall of the container. For ideal coupling, it was then filled completely with deionized water. All phantoms and *ex vivo* samples were imaged with a hybrid ultrasound MSOT system (MSOT Acuity Echo prototype imaging system, iThera Medical GmbH, Munich, Germany) described below.

Porcine DMD model

All animal experiments were performed in accordance with the German Animal Welfare Act and were approved by the responsible animal welfare authority (District Government of Upper

Bavaria, Reference Number 55.2-1-54-2532-163-2014). A heterozygous female carrier pig with a deletion of DMD exon 52 (*DMD*Δ52) was established by somatic cell nuclear transfer (SCNT) using primary cells with one modified DMD allele [9,37]. A breeding herd for DMD pigs was founded on heterozygous $DMD^{+/-}$ sows, generated by inseminating the founder animal with sperm from WT boars (Prüf- und Besamungsstation München Grub e.V., Munich, Germany). For the proof of concept study, male $DMD^{Y/-}$ piglets were selected as study subjects from three different litters, derived from matings of F1 $DMD^{+/-}$ pigs with wild-type boars at the Center for Innovative Medical Models (CiMM, LMU Munich, Germany). For the longitudinal porcine studies, male $DMD^{Y/-}$ piglets from two different litters were selected from matings of F2 $DMD^{+/-}$ pigs as described above.

Genotype Screening

Genotyping of piglets was carried out by polymerase chain reaction (PCR) analysis of DNA isolated from individual tail biopsies. The abundance of the intact (WT) DMD allele was detected by the primer pair 5´-tgc aca atg ctg gag aac ctc a-3´ and 5´-gtt ctg gct tct tga ttg ctg g-3´, whereas the mutated (*DMD*Δ52) allele was detected by the primer pair 5´-cag ctg tgc tcg acg ttg tc-3´ and 5´-gaa gaa ctc gtc aag aag gcg ata g-3´.

MSOT piglet imaging

For the proof-of-concept study, N = 17 piglets underwent standardized 2D MSOT-imaging by transversal scans of the shoulder (*triceps brachii muscle*) and the leg/thigh (*biceps femoris muscle*) muscles. All animals were scanned within 1 - 3 days after birth. N = 11 piglets were included in the longitudinal porcine pilot study. Here, all animals underwent standardized

transversal, and 3-dimensional imaging of the shoulder and leg/thigh muscles of both sides (**Fig. 6c** and **Supplementary appendix Table 21)**. Imaging was performed in week 1 (day 1-2), week 2 (day 2-3), week 3 (day 8/9), and week 4 (day 22/23) of life. Only WT piglets were sedated with intranasal application of Midazolam if required from week 2 onwards. DMD piglets were trained by LMF, and no sedation was required during MSOT imaging. All imaging investigators (AR, FK) were blinded to the genotype.

Histological examination and collagen quantification

In the proof of concept study, N = 9 animals (N = 6 WT and N = 3 DMD piglets) were euthanized 3-8 days after birth and representative tissue specimens were taken from the previously imaged anatomical regions. In the longitudinal study, N =10 animals (N = 5 WT and N = 5 DMD piglets) were examined after death; N = 5 in week 1 (N = 3 WT and N = 2 DMD), N = 5 in week 4 (N = 2 WT and N = 3 DMD). One WT was excluded from histological analysis, due to unknown exact time of death.

After harvesting, tissue was fixed in a 4% formaldehyde/phosphate buffered saline solution (Roti Histofix 4%; Carl Roth GmbH, Germany), and later embedded in paraffin. Sections (4µm thick) were stained with hematoxylin-eosin (H&E), Sirius Red (SirR), and Masson trichrome (TriC) according to standard laboratory protocols. Dystrophin immunohistochemistry was performed on sections of formalin-fixed, paraffin-embedded samples of the biceps femoris and triceps brachii muscle of a WT and a DMD piglets. Heat-induced antigen retrieval was performed using 10 mM citrate buffer (pH 6.0/0.05% Tween). Primary antibody was mouse monoclonal antibody against DYS1 (Rod domain) (dilution 1:20; overnight at 4°C; #NCL-DYS1; Clone: Dy4/6D3; Leica Biosystems), secondary antibody was biotinylated goat anti-mouse IgG (dilution 1:500; 1 hour at

room temperature; #115-065-146, Jackson ImmunoResearch). Bound antibodies were detected using the Vectastain Elite ABC HRP Kit (#PK-6100; Vector Laboratories) and 3,3-diaminobenzidine tetrahydrochloride dihydrate (#SK-4105; Vector Laboratories) as chromogen (brown color). Hemalaun was used as counterstain (blue color).

SirR and TriC stained sections were analyzed for their collagen content as following: histological sections were photographed with an AXIO Scope.A1 (Carl Zeiss AG, Germany) using AXIO Vs40 software (Version 4.8.10, Carl Zeiss Imaging Solutions GmbH) with 10-fold magnification. TIF files (1388x1040 pixels) were exported and analyzed using FIJI software (Version 2.0.0 or newer, available at https://fiji.sc) [61]. Then, the images were split in three channels (red, blue, and green). For collagen quantification in TriC, the red channel was used and for SirR staining the green channel was used. The respective positive stained tissue was calculated as a fraction from the whole images.

Collagen and protein assays

For total collagen (hydroxyproline) and total protein quantification, five paraffin embedded muscle tissue sections (10µm thick) per muscle were analyzed using a Total Collagen Assay (QuickZyme, Biosciences, Leiden, Netherlands) and a Total Protein Assay (QuickZyme, Biosciences, Leiden, Netherlands). According to manufacturer's instructions, the tissue was acidic hydrolyzed (6M HCl, Sigma-Aldrich Chemie GmbH, Steinheim, Germany, overnight at 95 °C). The samples for total collagen and total protein content were measured using a microplate reader (ELx808, BioTek, Winooski, US) at 550 nm. The absolute collagen content was derived from the quotient between total collagen and total protein.

Quantitative proteome analysis of skeletal muscle samples

Frozen tissue samples were cryopulverized using a cryoPREP hammer (Covaris, model no. CP02 cryoPREP Impactor) at an impact level of five. Tissue powder was homogenized in lysis buffer (8 M urea/0.4 M NH_4HCO_3) by ultrasonification (11 kJ, Sonopuls GM3200 equipped with a BR30 cup booster). Pierce 660 nm Protein Assay (Thermo Fisher Scientific) was used for total protein quantification. 60 µg of protein was reduced using dithiothreitol (DTT, final concentration 4 mM) for 30 min at 56 °C and cysteines were alkylated with iodoacetamide (IAA, final concentration 8 mM) for 30 min in the dark. Residual IAA was quenched with DTT at a final concentration of 10 mM during 15 min incubation in the dark. Proteins were digested with Lys-C (Wako Chemicals) at an enzyme/substrate ratio of 1:50 for 4 h at 37 °C. Samples were diluted with water to 0.8 M urea and digested overnight at 37 °C with trypsin (1:50; Promega). Nano-LC-MS/MS analysis was conducted on an Ultimate 3000 nano-LC system (Thermo Fisher Scientific) coupled online to a Q Exactive HF-X mass spectrometer (Thermo Fisher Scientific). 1.5 µg of tryptic peptides were separated at 250 nL/min on a 50 cm column (PepMap RSLC C18, 75 µm ID, 2 µm, Thermo Fisher Scientific) from 5% to 25% solvent B (0.1% formic acid in acetonitrile) in 160 min and from 25% to 40% B in 10 min. Spectra were acquired by one full scan (350 to 1600 m/z) with a resolution of 60,000 and up to 15 data-dependent MS/MS scans with a resolution of 15,000. MS raw data were processed using MaxQuant (v. 1.6.7.0) [62] with FDR < 0.01 at the peptide and protein level. For protein identification, the NCBI RefSeq Sus scrofa database (v. 3-5-2019) was used. Label-free peptide and protein quantifications were performed by MaxQuant with the normalization feature disabled. Downstream data analysis and visualization was performed using Perseus (v. 1.6.7.0) [63] and R [64] as previously described [65].

Study design of pediatric MSOT study

All patients were recruited at the Department of Pediatric Neurology of the University Hospital of Erlangen between June 6th 2018 and June 15th 2018. Ten boys between 3 and 10 years of age with DMD, confirmed either by genotyping or biopsy, and with preserved walking ability, were enrolled in the study. As controls, ten sex- and age-matched, healthy volunteers (HV) were recruited during the same time period. HV with any pre-existing muscular disorder were excluded. After screening for study inclusion, all participants underwent physical examination, (standard) B-mode ultrasound and MSOT. Data collection included demographic and clinical features such as age, sex, height and weight as well as disease-specific characteristics such as disease duration and current treatment. The study was performed in accordance with the Declaration of Helsinki. Approval from the local ethics committee (Friedrich-Alexander-University of Erlangen-Nuremberg) was granted and written informed consent was obtained from parents/guardians. The study was registered at clinicaltrials.gov (ID: NCT03490214). For any identifiable images of research participants, written permission to publish was obtained.

Physical examinations

Patients and healthy volunteers underwent physical examination during the course of the study by three well-trained physiotherapists. All participants started with the 6-MWT[20,21], followed by timed function tests (rise from chair, rise from supine, 10 m walk/run, 4 stairs climb, 8 stairs climb and sit to stand-test) and manual muscle testing (MRC of 20 muscles/groups including shoulder, arm, hand, fingers, limb, leg, toes, head and trunk (grading 0-5)).[10,66-68]

In detail, the respective test was performed and scored as follows: 6-MWT=6-minute-walk-test (measures walking distance within six minutes; range: 0-theoretically infinite; lower distance

represents a higher degree of muscle function loss)[20,21], sit to stand-test (measures repetitions to rise from chair in one minute; one repetition to theoretically infinite; high number of repetitions indicate a better degree of muscle function and a lower degree of dyspnea; few repetitions indicate a higher degree of muscle function loss and a higher degree dyspnea) adapted from[67], rise from chair/supine (measures time to rise from chair in seconds; 0.5 seconds to a time limit of 120 seconds; short time indicates a better degree of muscle function; long time indicates a higher degree of muscle function loss)[10,66,68], 10-meter walk/run (measures time to run 10 meters in seconds; a few seconds to a time limit of 120 seconds; short time indicates a better degree of muscle function; long time indicates a higher degree of muscle function loss)[10,66,68], 4-/8-stairs climb (measures time to climb 4 stairs in seconds; a few seconds to a time limit of 120 seconds; short time indicates a better degree of muscle function; long time indicates a higher degree of muscle function loss)[10,66,68], manual muscle testing of 20 muscles using the Medical Research Council (MRC) strength grading system; grade 0-5 (0=paralysis to 5=full strength).[10,66,68] For statistical analysis the muscles were grouped in 4 anatomical regions (proximal and distal muscles of the upper and lower extremity) and a mean muscle-strength-score was calculated for each region. Duration for physical examination was limited to one hour. Missing data points were excluded from final analysis.

MRI acquisition and analysis

N = 5 DMD patients of our study were simultaneously recruited by the Radiology Department of the University Hospital Erlangen in a separate study for an analysis of ^{23}Na MRI to detect early changes in ion homeostasis in DMD patients between February 2018 to May 2018. The study was approved by the local Ethical Review Board (Number: 250_16 Bc). MR data acquisition

methods have been described previously [18]. Briefly, all participants underwent MRI (Magnetom Skyra, 3 T, Siemens Healthineers, Erlangen, Germany) of their right lower leg. The imaging protocol consisted of a ^{1}H MRI part (using a dedicated 15-channel knee coil (Siemens Healthineers, Germany)) and a ^{23}Na MRI part (using a dedicated 1-channel knee coil (Stark Contrast, Germany). Details of the protocol are displayed in the **Supplementary Table 22**. Fat fraction (FF) and water T2 maps were obtained from the ^{1}H protocol as well as total sodium concentration (TSC) and intracellular-weighted sodium signal (ICwS) maps from the ^{23}Na protocol. ROIs for ^{23}Na MRI evaluation were drawn on anatomical reference images and interpolated on the sodium maps. For MRI imaging analysis, manually drawn ROIs were placed in the gastrocnemius muscles corresponding to MSOT images **(Figure 5b)**. All MRIs were reviewed by researchers with at least five years of experience (AMN and TG).

Analysis of ^{23}Na MRI in comparison to MSOT in DMD patients

A retrospective comparative analysis of MRI and MSOT was conducted to correlate the respective information. The median of five MRI sections (10mm width, each) was used for the analysis of water T_2 maps and FF; TSC and ICwS signals were evaluated from corresponding sections (15mm and 20mm width, respectively). For comparison between MRI and MSOT collagen and fat parameters, transversal 2D MSOT images were used.

MSOT and ultrasound imaging standardization

All patients and healthy controls underwent MSOT and ultrasound imaging of eight predefined anatomical regions (biceps brachii muscle, anterior forearm flexors, rectus femoris muscle and gastrocnemius muscle; both sides). Posture and detector (2D/3D MSOT detectors, ultrasound

detector) placement were standardized and marked to ensure scanning reproducibility for all imaging devices (for details see **Supplementary Table 23/Extended Data Fig. 7**).

B-mode ultrasound technical data

All anatomical regions were scanned using a single high-end ultrasound system (Logiq L9, General Electric Company, Milwaukee, Wisconsin, USA, Linear probe M12L, 9 MHz) by a single, professional investigator (certification level: DEGUM III). The ultrasound datasets were saved as raw data (DICOM). Echogenicity (hyper-/iso-/hypo-echogenic), Heckmatt-Scale (1-4)[69], muscle-texture (coarse-/medium-/fine-granular) and the distribution pattern (in-/homogeneous/focal) were assessed for each image.[70] The total investigation time for ultrasound imaging was limited to twenty minutes.

MSOT technical data

All images were obtained with two separate hybrid ultrasound MSOT systems (MSOT Acuity Echo prototype imaging system, iThera Medical GmbH, Munich, Germany), one system was only used for piglets and one only for human imaging. The optoacoustic imaging system is based on a 25Hz pulsed Nd:YAG laser and has two detectors. The 2D concave handheld detector (4 MHz center frequency, 256 transducer elements) with a field of view of 30 mm and spatial resolution of <150µm provides cross sectional images and is combined with a reflective ultrasound computed tomography (RUCT) unit, to anatomically guide optoacoustic imaging during the examination. The 3D hemispherical handheld detector (8 MHz center frequency, 256 transducer elements) with a field of view of 15 mm and a spatial resolution of 100 µm provides

isotropic volumetric optoacoustic images. Transparent ultrasound gel (AQUASONIC clear®, Parker Laboratories Inc., Fairfield, NJ, USA) was used for coupling between detector and skin. For the phantom and *ex vivo* experiments, Multispectral optoacoustic tomography signals were acquired from 660 nm to 1200 nm in 5 nm steps. For *in vivo* imaging, Multispectral optoacoustic tomography signals were acquired at 680, 700, 730, 760, 800, 850, 920, 1000, 1030, 1064, and 1100 nm. A polygonal region of interest was placed just beneath the muscle fascia according to the MSOT-signal.

MSOT data analysis

2D imaging data was analyzed using cLabs software (Version 2.66, iThera Medical GmbH, Munich, Germany). The program enables analysis of user-defined MSOT parameters (in arbitrary units, a.u.) and extraction of optoacoustic spectra from the region of interest in the multispectral optoacoustic images. 3D imaging data was analyzed using ViewMSOT software (Version 3.8, iThera Medical GmbH, Munich, Germany). MSOT data were reconstructed with direct backprojection and spatial fluence correction was applied for images acquired with the 2D detector (μ_a=0.022 and μ_s=10cm^{-1}). Using spectral unmixing, MSOT values for Hb_R, HbO_2 and collagen were obtained. Collagen unmixing was based on acquired wavelengths of the entire spectral range, whereas Hb_R, HbO_2 signal was calculated from a sub-range (730 nm and 850 nm) which is more accurate in unmixing due to increase of water absorptivity at higher wavelengths. Single wavelength of 920 nm was used to depict lipid signals. To aid interpretation, 3D signals (a.u.) were rescaled: human collagen signals (a.u.) were multiplied by 10^4 and hemoglobin signals (a.u.) were multiplied by 10^7; piglet $collagen_{mean}$ signals (a.u.) were multiplied by 10^4 and $collagen_{max}$ signals by 10^3.

Device tolerability

The imaged skin of every participant was visually examined after each scan. Investigated subjects and parents/guardians were asked about any inconvenience during the imaging sessions/trials. All reported events were documented.

Statistical analysis

Due to the study design (pilot first-in piglet, first-in pediatric, first longitudinal *in vivo* use of MSOT, no former description of collagen signal derived from MSOT *in vivo*) no sample size calculation was performed. For piglets, the sample size corresponded to three litters for the proof of concept, and two litters for the longitudinal porcine pilot trial. Ten Duchenne patients and healthy volunteers were found to be reasonable and ethically justified for the patient study. Continuous variables are given as means and standard deviations; categorical variables are provided as numbers and percentages. Data were tested for normal distribution using Shapiro-Wilk test prior to inferential analysis. Between piglet group comparisons (DMD vs. WT) of MSOT parameters and histological results were conducted using independent samples t-tests. In case of unequal variances in an independent samples t-tests, Welch's correction was applied. If the assumption of normal distribution was violated, a Mann-Whitney U-test was chosen for the independent samples comparison. Correlations are given by Spearman correlation coefficient (r_s). Human MSOT parameters were compared between cohorts in a pairwise manner (matched for age) using dependent samples t-tests. If the assumption of normal distribution was violated Wilcoxon signed-rank tests was used. We performed receiver operator characteristics (ROC) analysis between muscles of WT/HV and DMD-piglets/DMD-patients. As gold standard

histopathology and genotyping were used. Wilcoxon signed-rank tests were used for comparison of physical examinations. For comparison of the duration of examinations, Mann-Whitney U-tests were applied. For longitudinal comparisons of 3D MSOT collagen parameters in the porcine pilot trial, Tukey's honestly significant difference tests following a two-way (mixed design) ANOVA including piglet group and time points were chosen. For longitudinal comparison of 2D MSOT parameters, post-hoc Tukey's HSD following a mixed-effects models (fixed effects: piglet group & time points, random effect: piglet) were used due to missing values in week 1 (litter 1)). Independent samples t-tests were applied to compare all scans of WT and DMD piglets at each week. In case of unequal variances in an independent samples t-tests, Welch's correction was applied. If the assumption of normal distribution was violated, a Mann-Whitney U-test was chosen for the independent samples comparison. Quantitative proteome analysis was performed as described above. All inferential tests were two-tailed, p values ≤ 0.05 were considered statistically significant. Bonferroni-Holm adjustment was used to control type I error. Complete information on inferential test results including test coefficient, p-value, and effect size are presented in the Supplementary Appendix. All analyses were performed using GraphPad Prism (Version 7.00 or newer, GraphPad Software, La Jolla, CA, USA).

Statistics and Reproducibility

MSOT signals were derived from averaged video captures (seven frames) obtained in anatomical independent muscle regions in piglets and patients. All anatomical locations were considered independent because of the heterogenicity of the underlying disease. In cases of multiple scans/recordings (e.g. because of piglet/patient movement), a mean of all scans was calculated. 2D transversal and 2D longitudinal MSOT scans at the same anatomical locations were

considered as technical replicates. As a consequence, all statistical analysis was based on one (transversal) imaging orientation. In order to provide a universal readout for each subject, a mean MSOT signal was calculated over all anatomical regions. This was used for correlations to clinical standard testing.

Data availability statement

The data sets generated during and/or analyzed during the current study are available from the corresponding author on reasonable request. Restrictions may apply due to patient privacy and the General Data Protection Regulation.

Methods-only references

61. Schindelin, J., *et al.* Fiji: an open-source platform for biological-image analysis. *Nat Methods* **9**, 676-682 (2012).
62. Cox, J. & Mann, M. MaxQuant enables high peptide identification rates, individualized p.p.b.-range mass accuracies and proteome-wide protein quantification. *Nat. Biotechnol.* **26**, 1367-1372 (2008).
63. Tyanova, S., *et al.* The Perseus computational platform for comprehensive analysis of (prote)omics data. *Nat. Methods* **13**, 731-740 (2016).
64. R Core Team. R: A Language and Environment for Statistical Computing. (R Foundation for Statistical Computing, Vienna, Austria, 2018).
65. Backman, M., *et al.* Multi-omics insights into functional alterations of the liver in insulin-deficient diabetes mellitus. *Mol Metab* **26**, 30-44 (2019).
66. Brooke, M.H., *et al.* Clinical trial in Duchenne dystrophy. I. The design of the protocol. *Muscle Nerve* **4**, 186-197 (1981).
67. Ozalevli, S., Ozden, A., Itil, O. & Akkoclu, A. Comparison of the Sit-to-Stand Test with 6 min walk test in patients with chronic obstructive pulmonary disease. *Respir Med* **101**, 286-293 (2007).
68. Fowler, W.M., Jr., *et al.* Profiles of neuromuscular diseases. Design of the protocol. *Am J Phys Med Rehabil* **74**, S62-69 (1995).
69. Heckmatt, J.Z., Leeman, S. & Dubowitz, V. Ultrasound imaging in the diagnosis of muscle disease. *J Pediatr* **101**, 656-660 (1982).
70. Pillen, S., Arts, I.M. & Zwarts, M.J. Muscle ultrasound in neuromuscular disorders. *Muscle Nerve* **37**, 679-693 (2008).

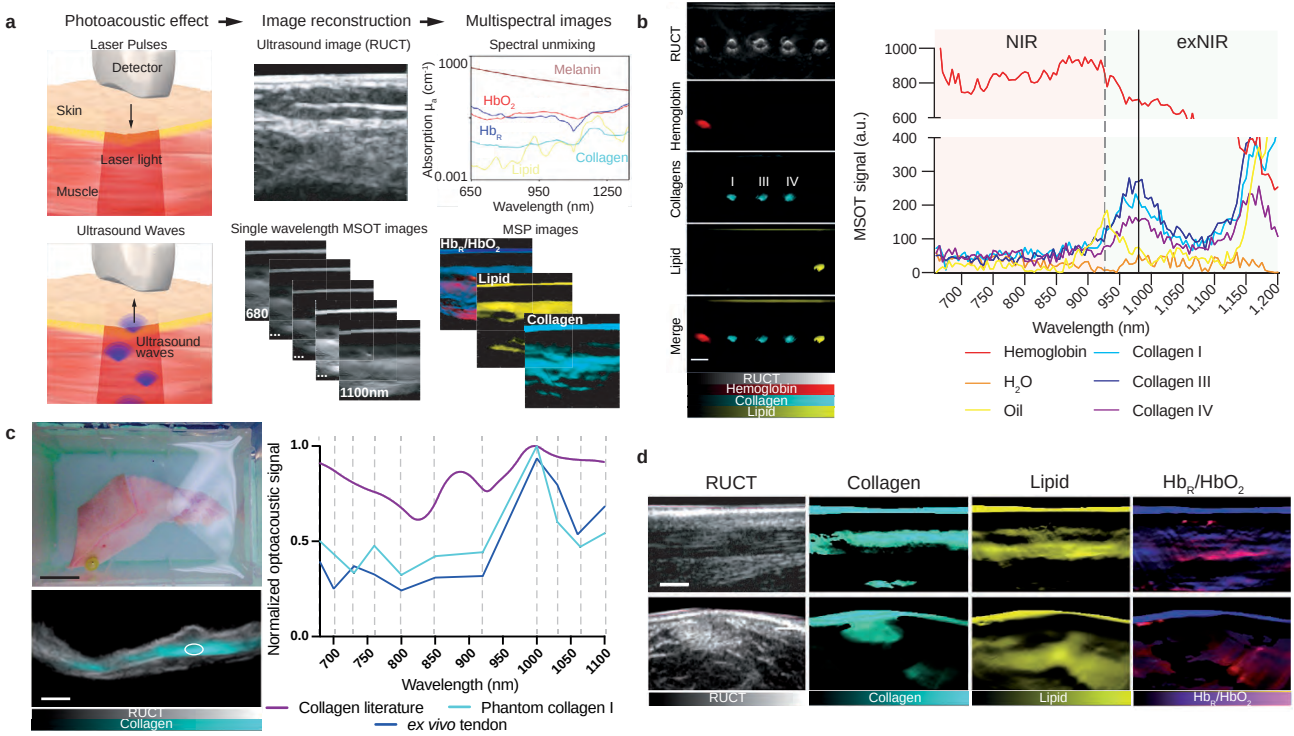
a
Photoacoustic effect
Image reconstruction
Multispectral images
Laser Pulses
Detector
Skin
Laser light
Muscle
Ultrasound image (RUCT)
Spectral unmixing
Melanin
HbO2
HbR
Lipid
Collagen
Absorption μa (cm-1)
1000
0.001
650
950
1250
Wavelength (nm)
Ultrasound Waves
Ultrasound waves
Single wavelength MSOT images
680
1100nm
MSP images
HbR/HbO2
Lipid
Collagen
b
RUCT
Hemoglobin
Collagens
I
III
IV
Lipid
Merge
RUCT
Hemoglobin
Collagen
Lipid
NIR
exNIR
MSOT signal (a.u.)
1000
800
600
400
300
200
100
0
700
750
800
850
900
950
1,000
1,050
1,100
1,150
1,200
Wavelength (nm)
Hemoglobin
H2O
Oil
Collagen I
Collagen III
Collagen IV
c
RUCT
Collagen
Normalized optoacoustic signal
1.0
0.5
0.0
700
750
800
850
900
950
1000
1050
1100
Wavelength (nm)
Collagen literature
Phantom collagen I
ex vivo tendon
d
RUCT
Collagen
Lipid
HbR/HbO2
RUCT
Collagen
Lipid
HbR/HbO2

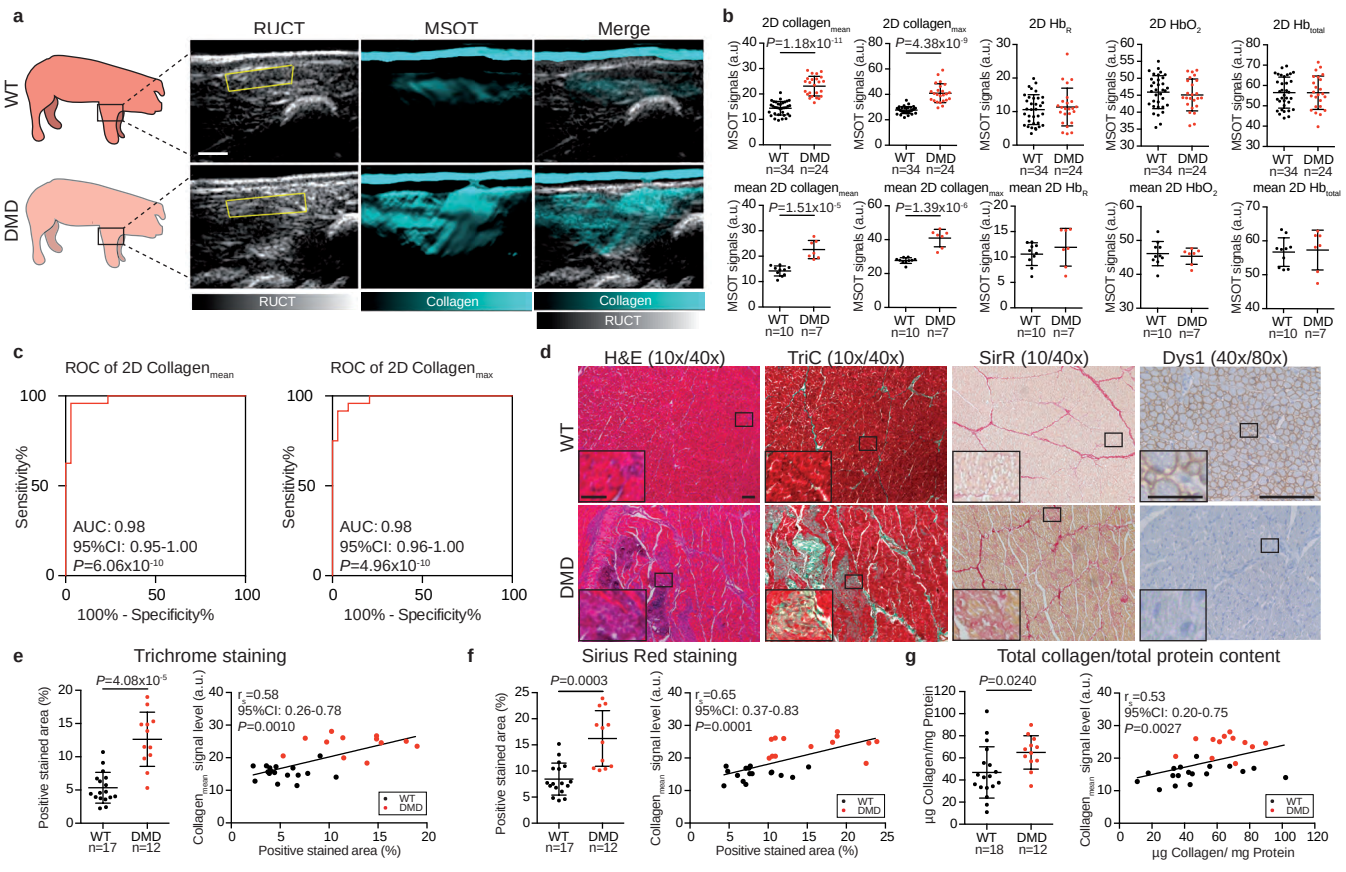
a
RUCT
MSOT
Merge
WT
DMD
RUCT
Collagen
Collagen
RUCT
b
2D collagen mean
2D collagen max
2D Hb R
2D HbO2
2D Hb total
P=1.18x10-11
P=4.38x10-9
MSOT signals (a.u.)
WT n=34
DMD n=24
mean 2D collagen mean
mean 2D collagen max
mean 2D Hb R
mean 2D HbO2
mean 2D Hb total
P=1.51x10-5
P=1.39x10-6
WT n=10
DMD n=7
c
ROC of 2D Collagen mean
ROC of 2D Collagen max
Sensitivity%
100% - Specificity%
AUC: 0.98
95%CI: 0.95-1.00
P=6.06x10-10
AUC: 0.98
95%CI: 0.96-1.00
P=4.96x10-10
d
H&E (10x/40x)
TriC (10x/40x)
SirR (10/40x)
Dys1 (40x/80x)
WT
DMD
e
Trichrome staining
P=4.08x10-5
Positive stained area (%)
WT n=17
DMD n=12
r=0.58
95%CI: 0.26-0.78
P=0.0010
Collagen mean signal level (a.u.)
Positive stained area (%)
f
Sirius Red staining
P=0.0003
r=0.65
95%CI: 0.37-0.83
P=0.0001
g
Total collagen/total protein content
P=0.0240
µg Collagen/mg Protein
WT n=18
DMD n=12
r=0.53
95%CI: 0.20-0.75
P=0.0027
µg Collagen/ mg Protein

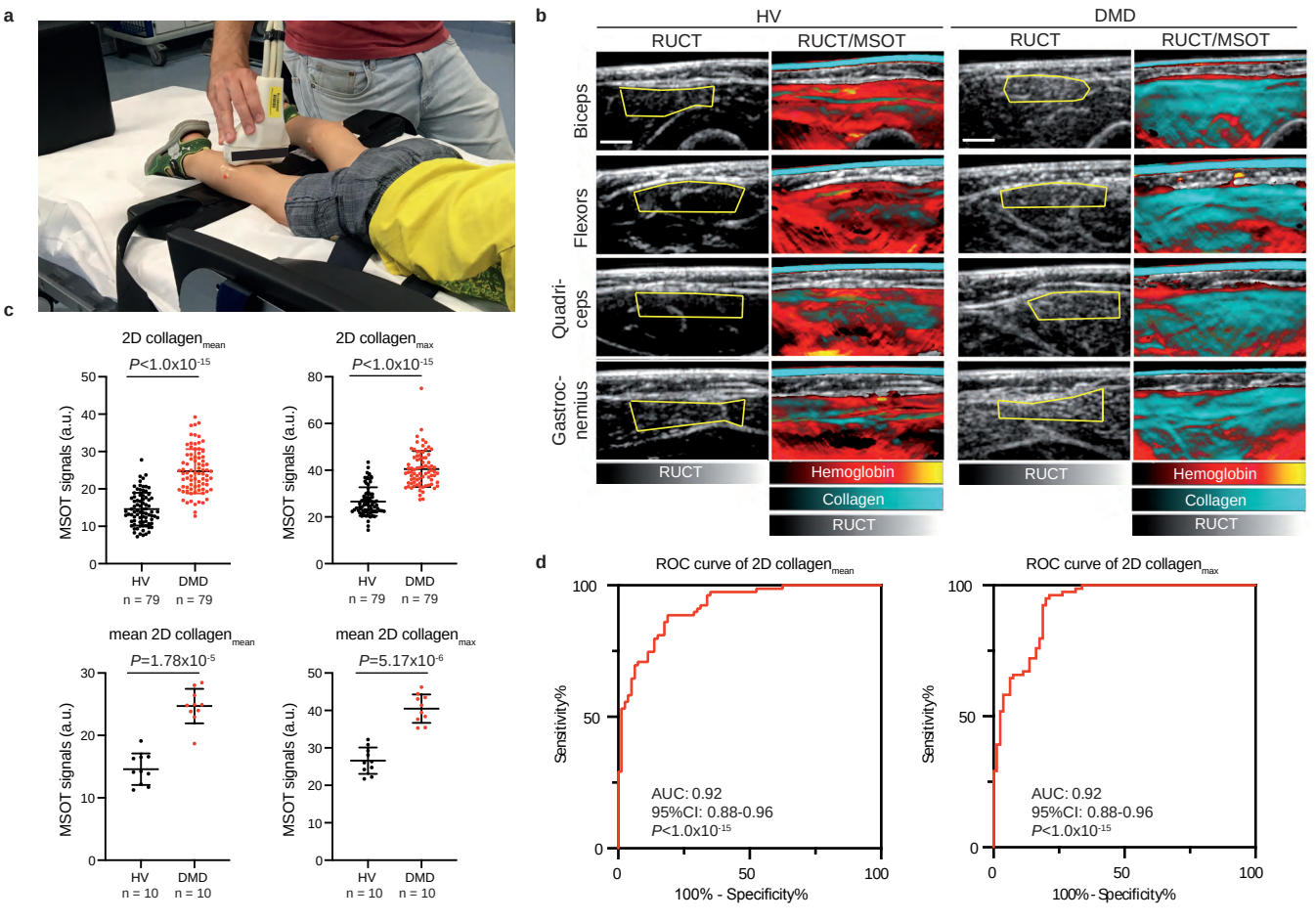
a
b
HV
DMD
RUCT
RUCT/MSOT
RUCT
RUCT/MSOT
Biceps
Flexors
Quadri-ceps
Gastroc-nemius
RUCT
Hemoglobin
Collagen
RUCT
RUCT
Hemoglobin
Collagen
RUCT
c
2D collagen mean
P<1.0x10-15
MSOT signals (a.u.)
HV
DMD
n = 79
n = 79
2D collagen max
P<1.0x10-15
MSOT signals (a.u.)
HV
DMD
n = 79
n = 79
mean 2D collagen mean
P=1.78x10-5
MSOT signals (a.u.)
HV
DMD
n = 10
n = 10
mean 2D collagen max
P=5.17x10-6
MSOT signals (a.u.)
HV
DMD
n = 10
n = 10
d
ROC curve of 2D collagen mean
Sensitivity%
100% - Specificity%
AUC: 0.92
95%CI: 0.88-0.96
P<1.0x10-15
ROC curve of 2D collagen max
Sensitivity%
100% - Specificity%
AUC: 0.92
95%CI: 0.88-0.96
P<1.0x10-15

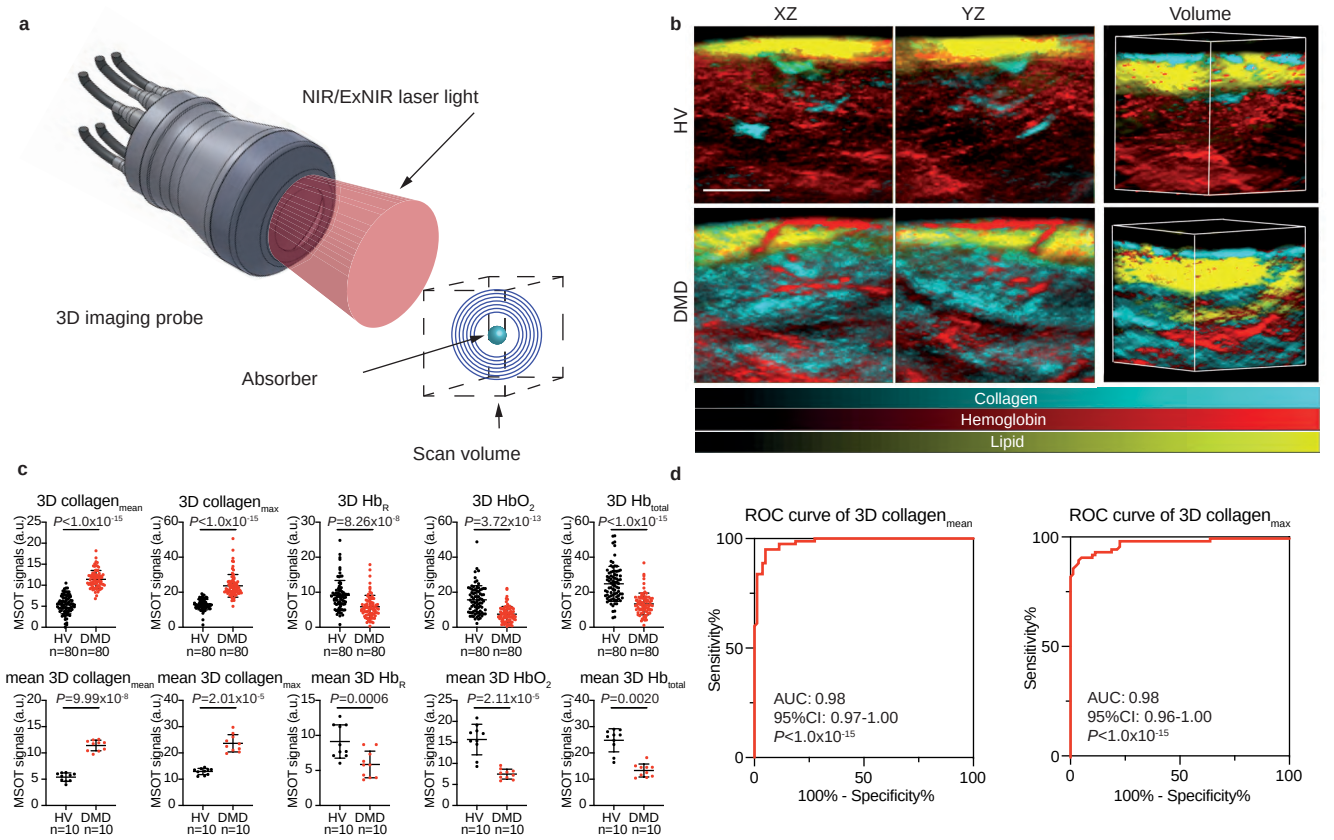
a
NIR/ExNIR laser light
3D imaging probe
Absorber
Scan volume
b
XZ
YZ
Volume
HV
DMD
Collagen
Hemoglobin
Lipid
c
3D collagen$_{mean}$
3D collagen$_{max}$
3D Hb$_R$
3D HbO$_2$
3D Hb$_{total}$
MSOT signals (a.u.)
P<1.0x10-15
P=8.26x10-8
P=3.72x10-13
HV DMD
n=80 n=80
mean 3D collagen$_{mean}$
mean 3D collagen$_{max}$
mean 3D Hb$_R$
mean 3D HbO$_2$
mean 3D Hb$_{total}$
P=9.99x10-8
P=2.01x10-5
P=0.0006
P=2.11x10-5
P=0.0020
n=10 n=10
d
ROC curve of 3D collagen$_{mean}$
ROC curve of 3D collagen$_{max}$
Sensitivity%
100% - Specificity%
AUC: 0.98
95%CI: 0.97-1.00
P<1.0x10-15
95%CI: 0.96-1.00

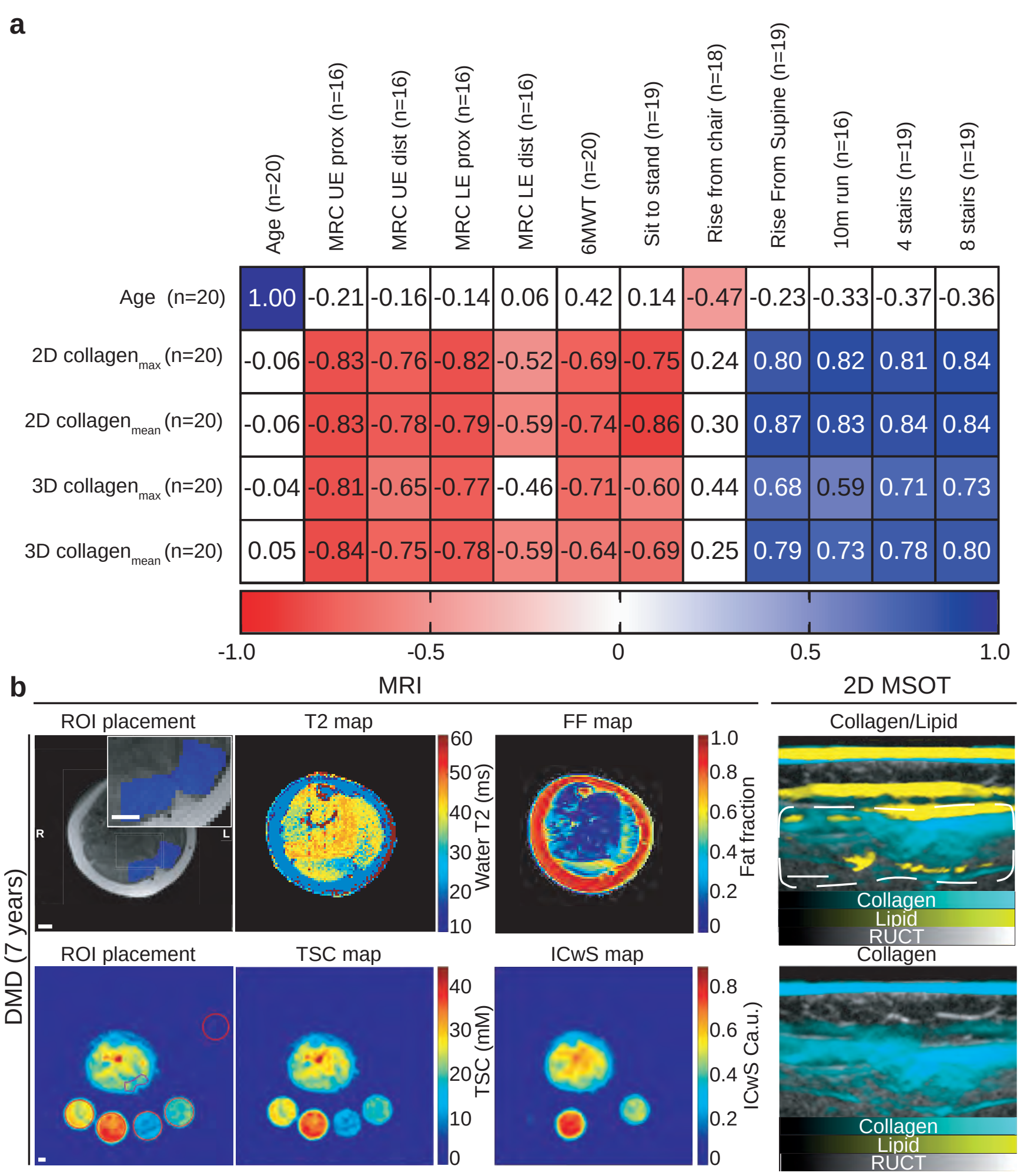
a
Age (n=20)
MRC UE prox (n=16)
MRC UE dist (n=16)
MRC LE prox (n=16)
MRC LE dist (n=16)
6MWT (n=20)
Sit to stand (n=19)
Rise from chair (n=18)
Rise From Supine (n=19)
10m run (n=16)
4 stairs (n=19)
8 stairs (n=19)
Age (n=20) 1.00 -0.21 -0.16 -0.14 0.06 0.42 0.14 -0.47 -0.23 -0.33 -0.37 -0.36
2D collagen max (n=20) -0.06 -0.83 -0.76 -0.82 -0.52 -0.69 -0.75 0.24 0.80 0.82 0.81 0.84
2D collagen mean (n=20) -0.06 -0.83 -0.78 -0.79 -0.59 -0.74 -0.86 0.30 0.87 0.83 0.84 0.84
3D collagen max (n=20) -0.04 -0.81 -0.65 -0.77 -0.46 -0.71 -0.60 0.44 0.68 0.59 0.71 0.73
3D collagen mean (n=20) 0.05 -0.84 -0.75 -0.78 -0.59 -0.64 -0.69 0.25 0.79 0.73 0.78 0.80
-1.0
-0.5
0
0.5
1.0
b
MRI
2D MSOT
ROI placement
T2 map
FF map
Collagen/Lipid
DMD (7 years)
R
L
60
50
40
30
20
10
Water T2 (ms)
1.0
0.8
0.6
0.4
0.2
0
Fat fraction
Collagen
Lipid
RUCT
ROI placement
TSC map
ICwS map
Collagen
40
30
20
10
0
TSC (mM)
0.8
0.6
0.4
0.2
0
ICwS Ca.u.)
Collagen
Lipid
RUCT

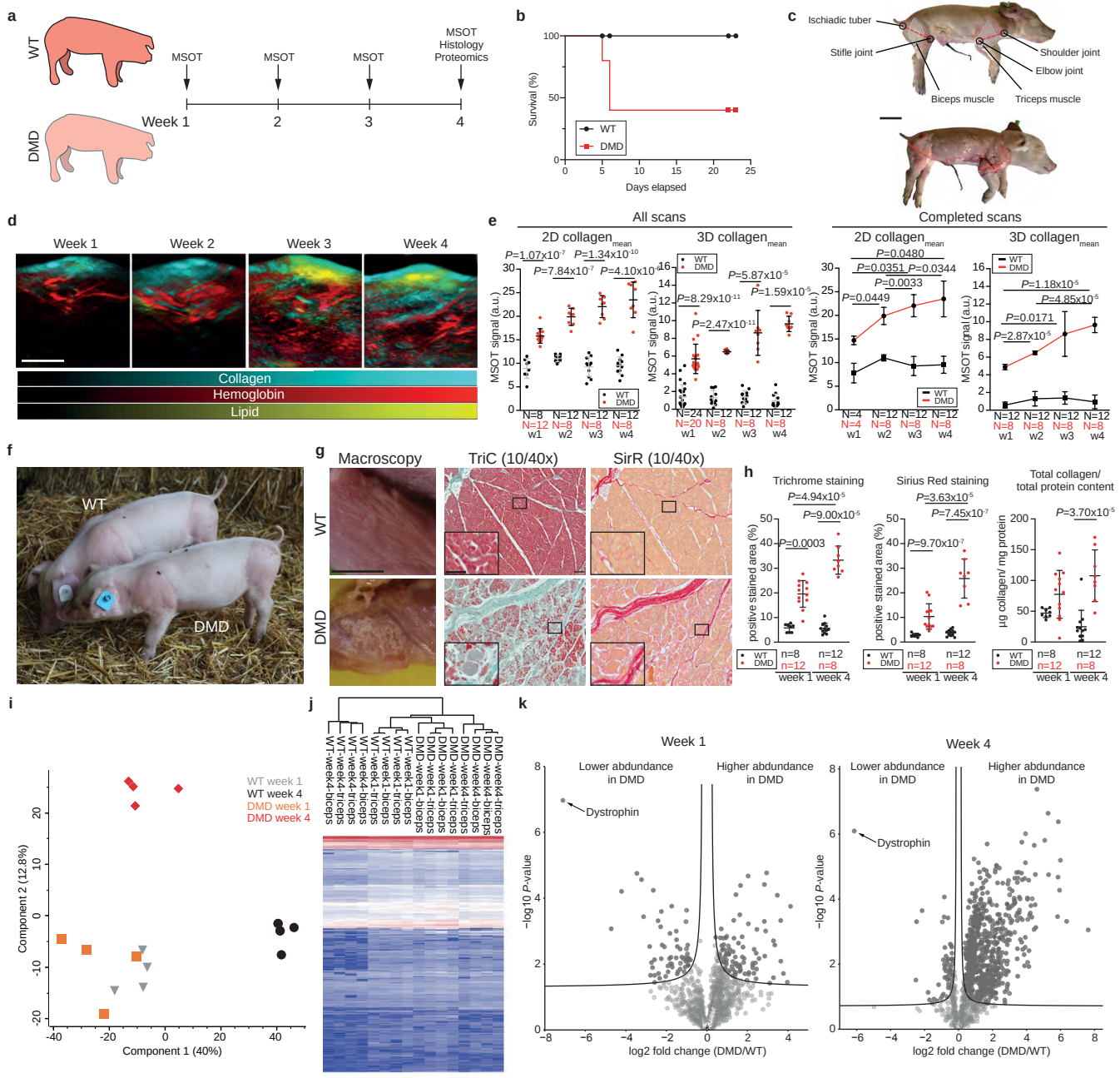
a
WT
DMD
MSOT
MSOT
MSOT
MSOT
Histology
Proteomics
Week 1
2
3
4
b
Survival (%)
Days elapsed
WT
DMD
c
Ischiadic tuber
Stifle joint
Shoulder joint
Elbow joint
Biceps muscle
Triceps muscle
d
Week 1
Week 2
Week 3
Week 4
Collagen
Hemoglobin
Lipid
e
All scans
Completed scans
2D collagen mean
3D collagen mean
MSOT signal (a.u.)
WT
DMD
f
WT
DMD
g
Macroscopy
TriC (10/40x)
SirR (10/40x)
WT
DMD
h
Trichrome staining
Sirius Red staining
Total collagen/ total protein content
positive stained area (%)
µg collagen/ mg protein
week 1 week 4
i
WT week 1
WT week 4
DMD week 1
DMD week 4
Component 1 (40%)
Component 2 (12.8%)
j
k
Week 1
Week 4
Lower abundance in DMD
Higher abundance in DMD
Dystrophin
−log10 P-value
log2 fold change (DMD/WT)

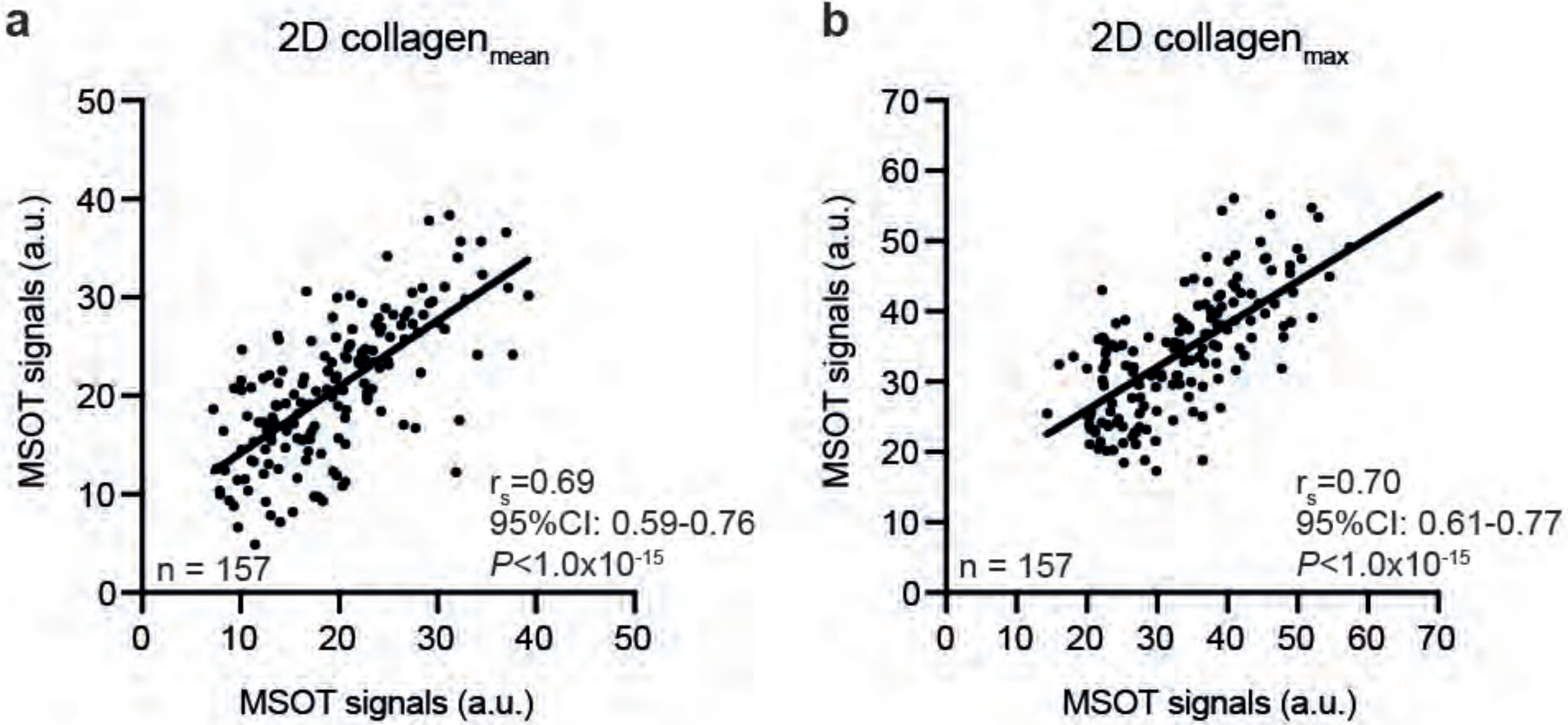
a
2D collagen mean
MSOT signals (a.u.)
MSOT signals (a.u.)
r s=0.69
95%CI: 0.59-0.76
P<1.0x10-15
n = 157
0
10
20
30
40
50
b
2D collagen max
MSOT signals (a.u.)
MSOT signals (a.u.)
r s=0.70
95%CI: 0.61-0.77
P<1.0x10-15
n = 157
0
10
20
30
40
50
60
70

transversal

longitudinal

HV

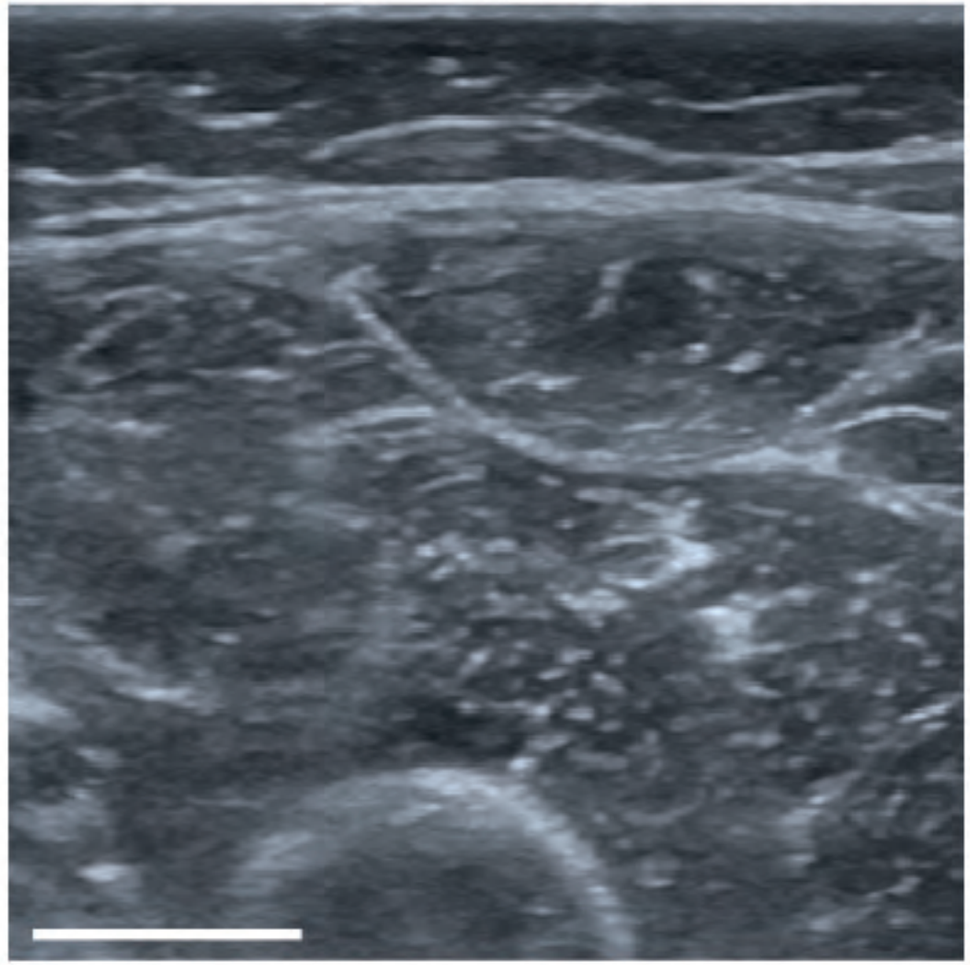

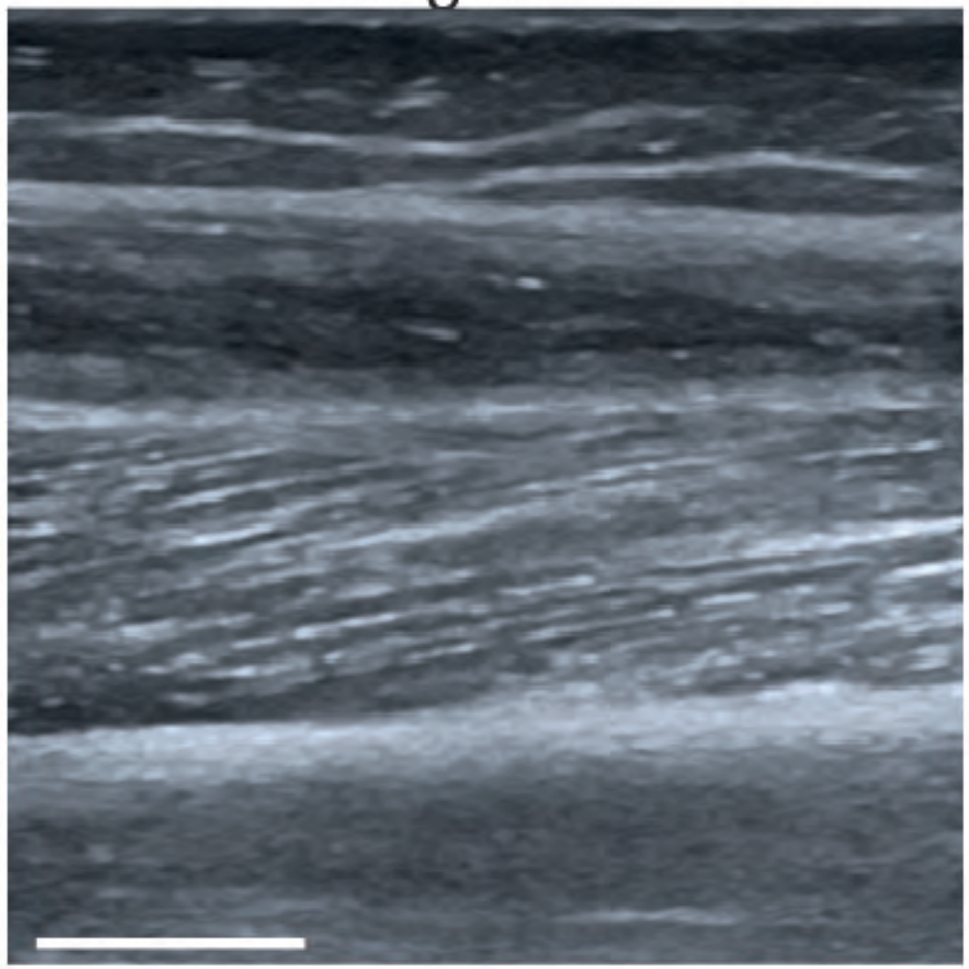

DMD

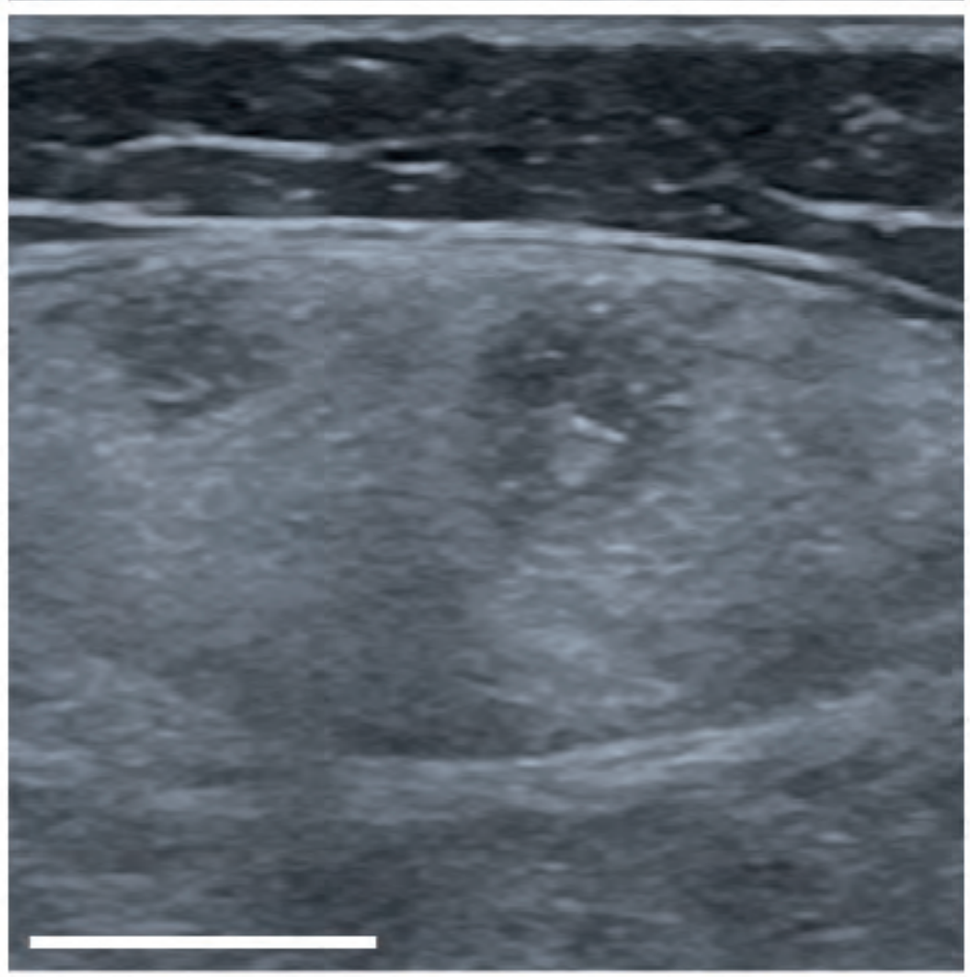

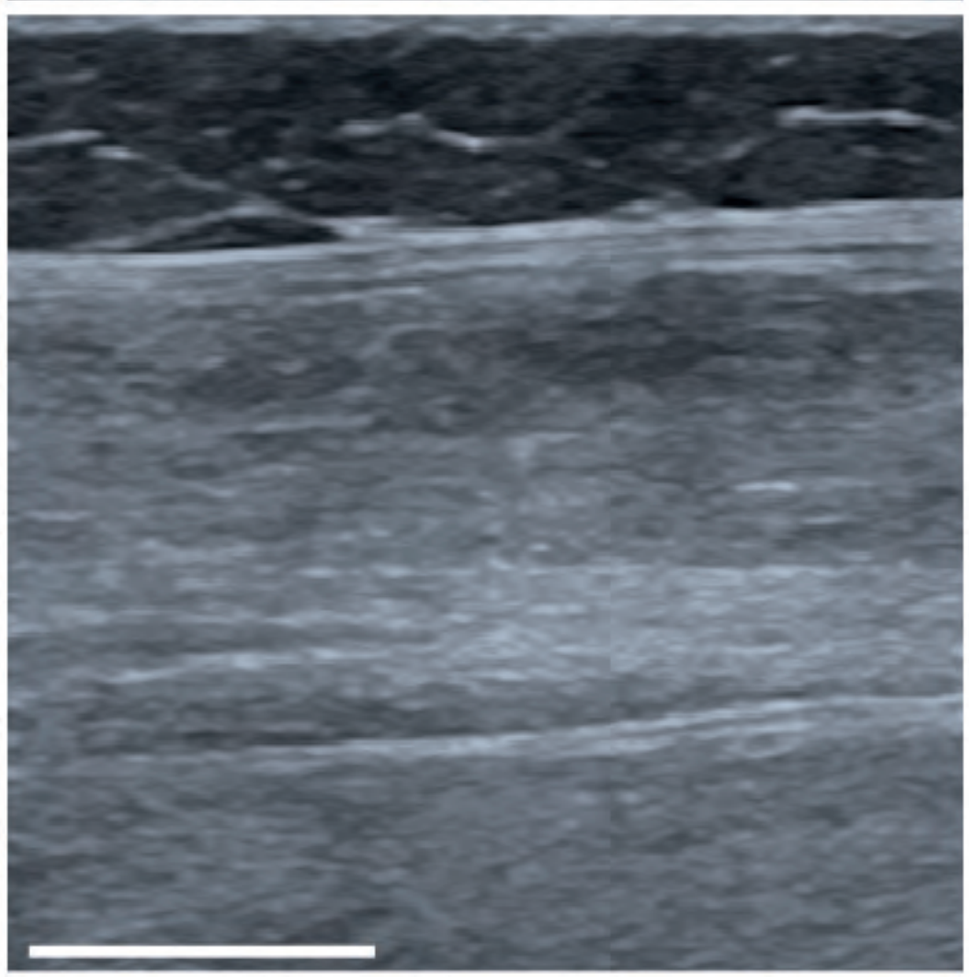

a

2D collagen$_{max}$

P=2.39x10^{-12}

P=6.47x10^{-6}

P=1.59x10^{-5}

P=1.59x10^{-5}

MSOT signal (a.u.)

40

30

20

10

0

WT

DMD

week 1 week 2 week 3 week 4

n=8 n=12 n=12 n=12

n=12 n=8 n=8 n=8

b

3D collagen$_{max}$

P=6.77x10^{-13}

P=4.74x10^{-9}

P<1.0x10^{-15}

P=4.81x10^{-8}

MSOT signal (a.u)

40

30

20

10

0

WT

DMD

week 1 week 2 week 3 week 4

n=24 n=12 n=12 n=12

n=20 n=8 n=8 n=8

a

2D collagen$_{max}$

P=0.0257

P=0.0273

P=0.0171

P=0.0088

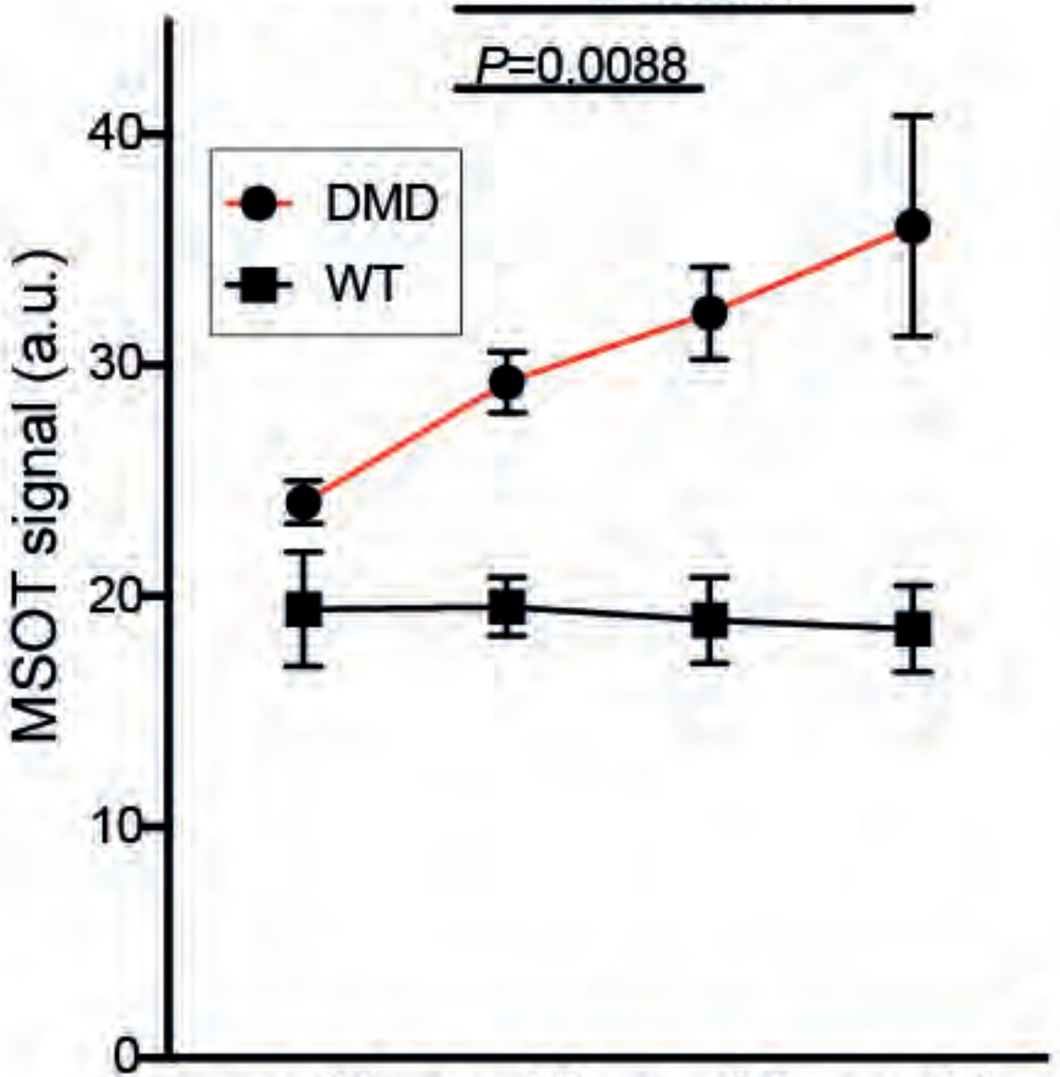

b

3D collagen$_{max}$

P=0.0019

P=0.0199

P=0.0011

P=0.0241

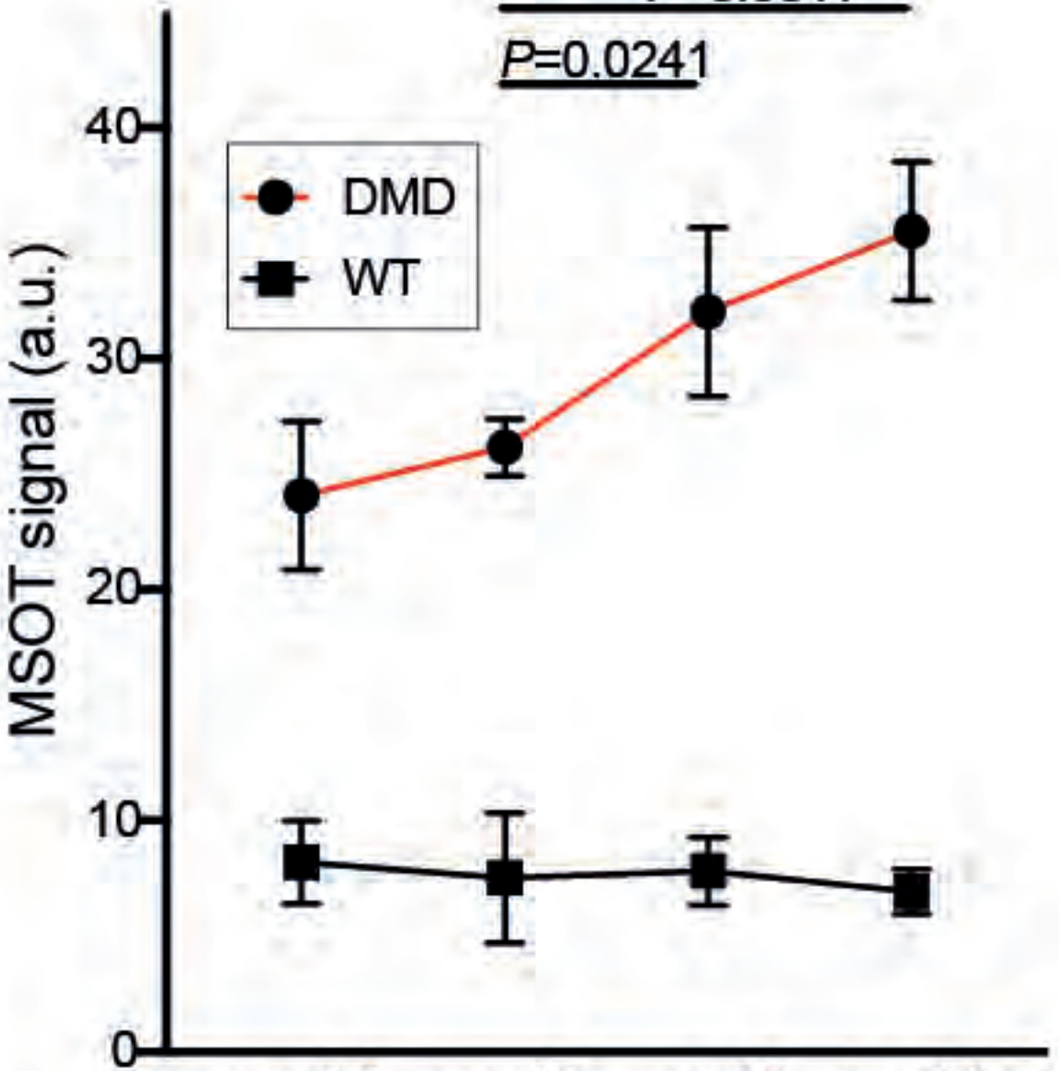

a

mean 2D collagen$_{mean}$

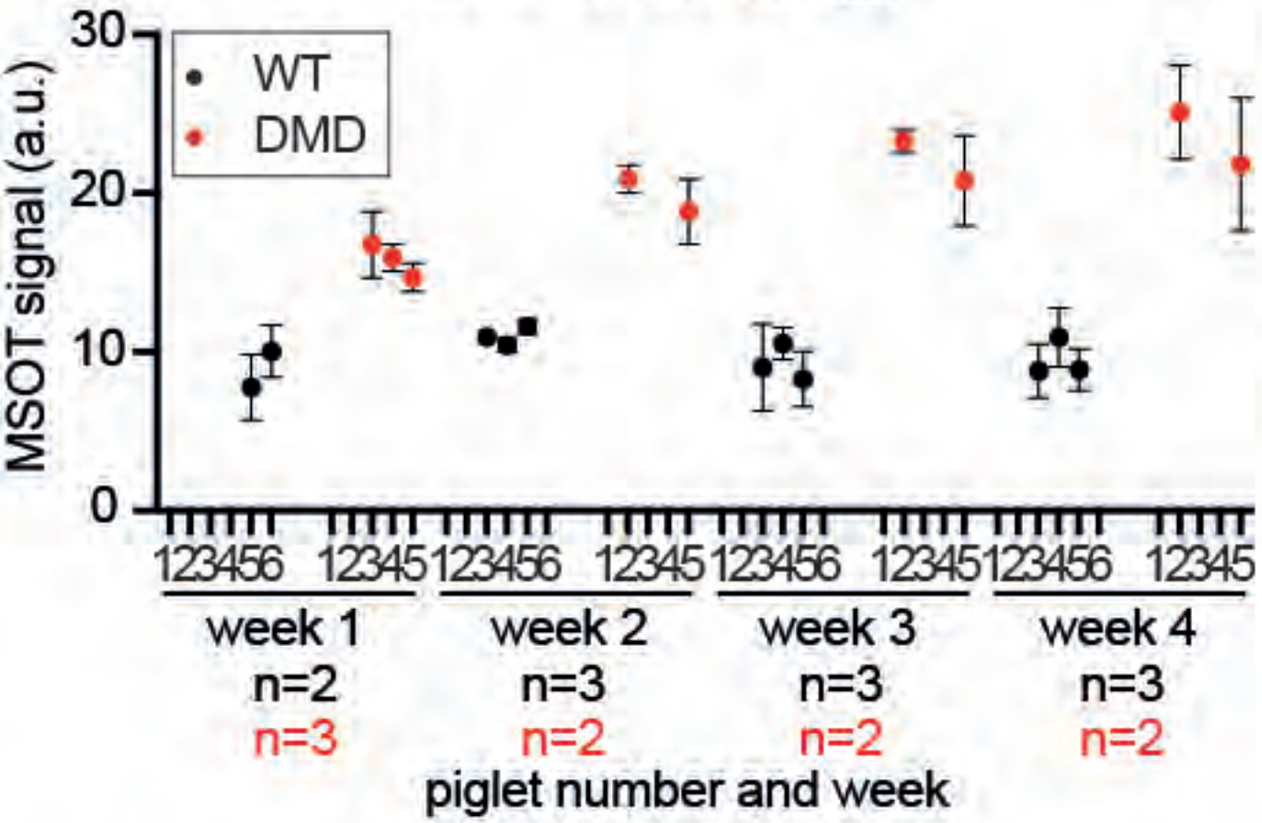

b

mean 2D collagen$_{max}$

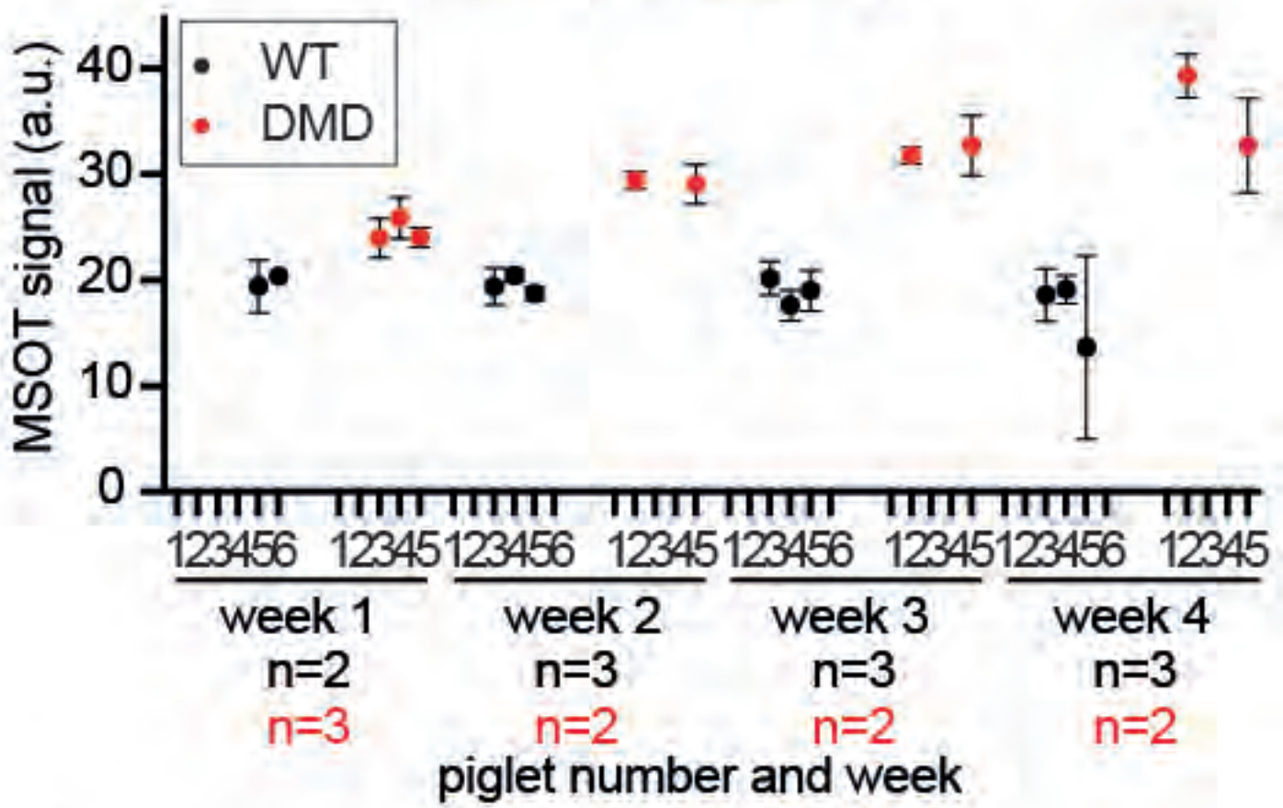

c

mean 3D collagen$_{mean}$

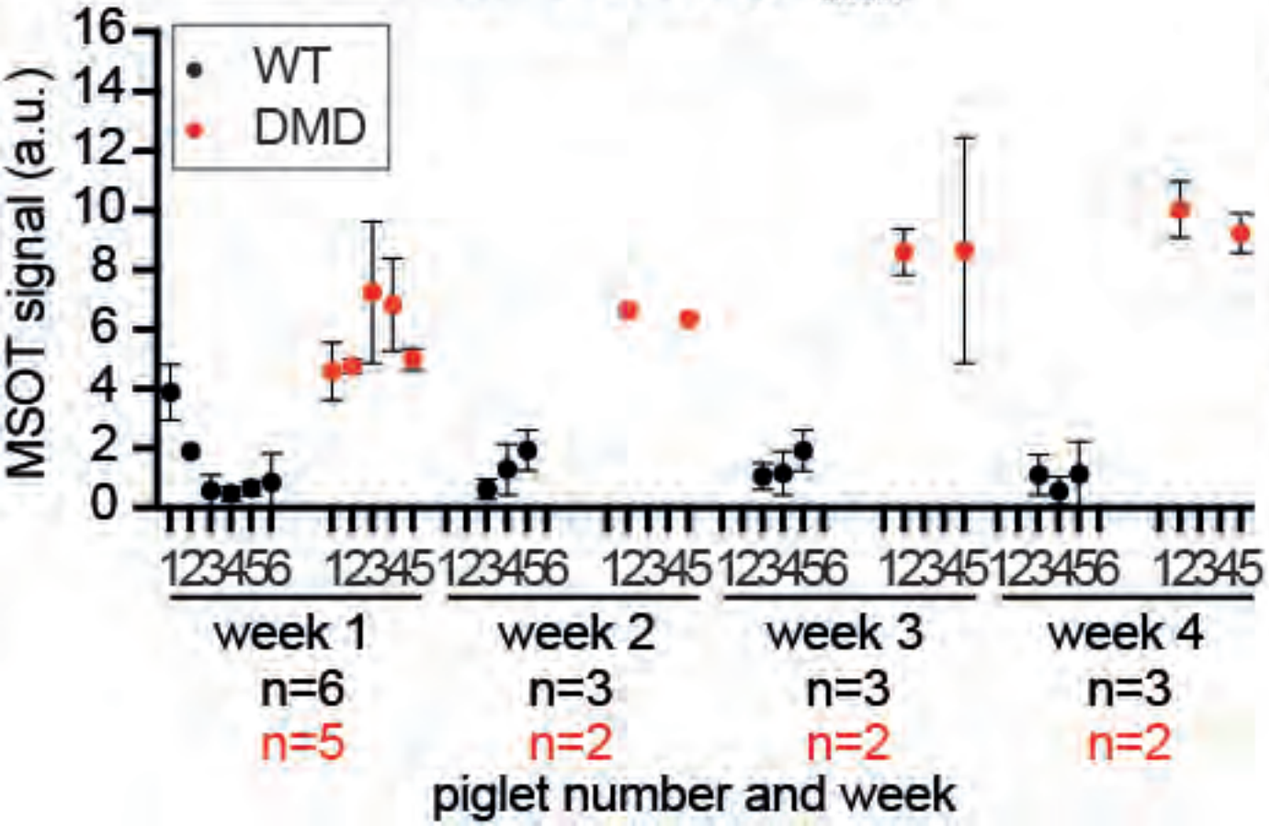

d

mean 3D collagen$_{max}$

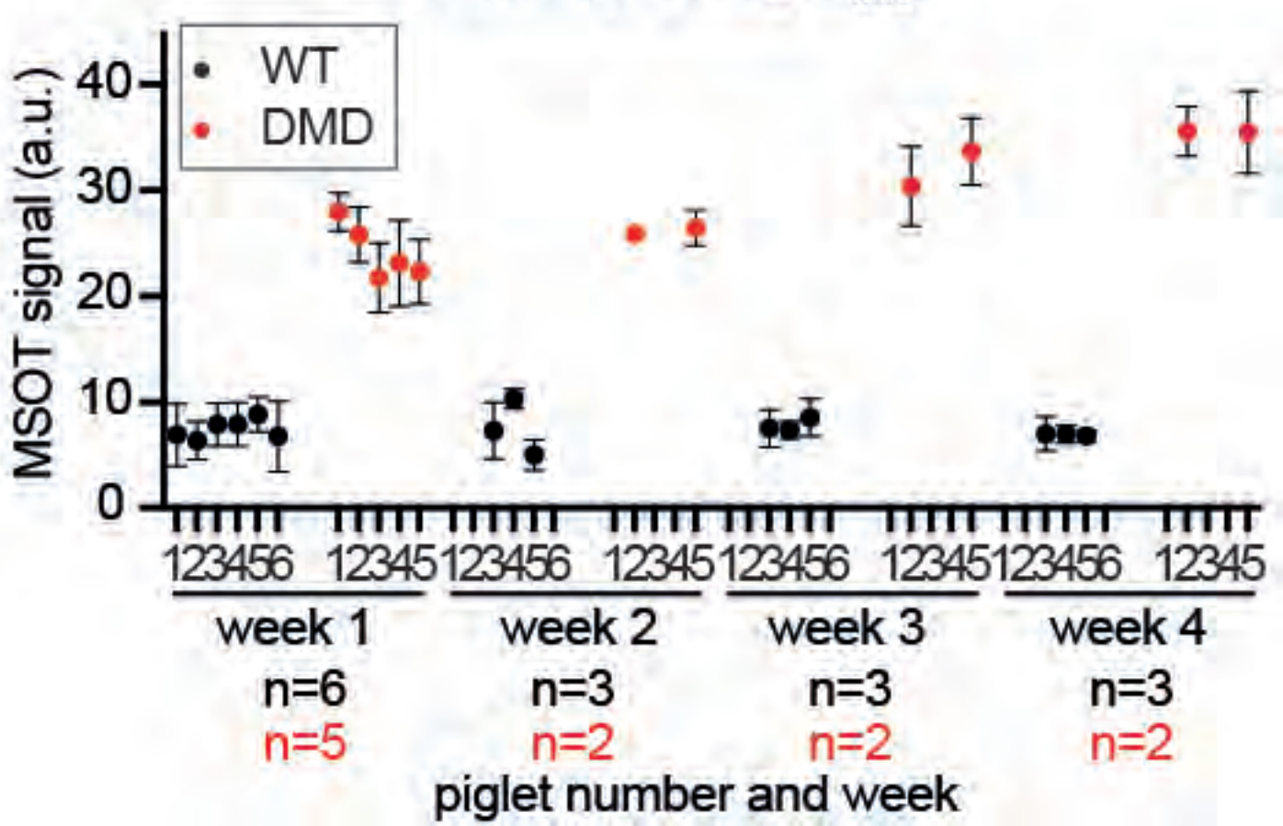

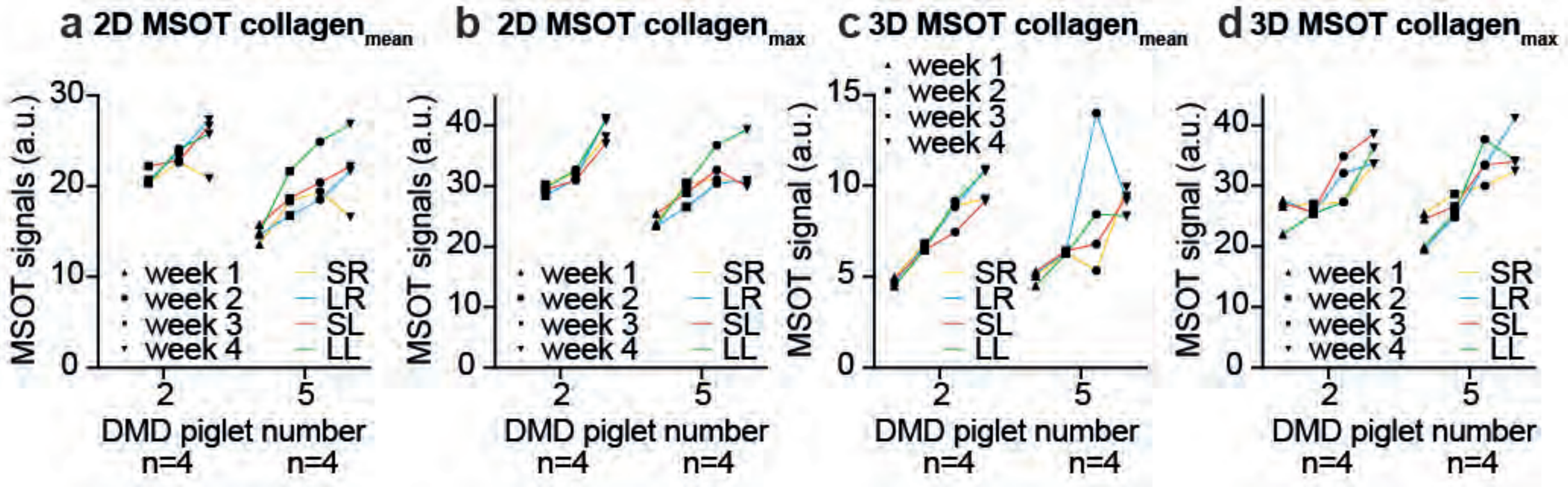
a 2D MSOT collagen mean
b 2D MSOT collagen max
c 3D MSOT collagen mean
d 3D MSOT collagen max
MSOT signals (a.u.)
MSOT signal (a.u.)
week 1
week 2
week 3
week 4
SR
LR
SL
LL
DMD piglet number
n=4
n=4